Technological impact on structure phase evolution of materials during irradiation

I.M. Neklyudov, V.N. Voyevodin

Department of Radiation Damage and Material Science,
National Science Center
"Kharkov Institute of Physics and Technology"

1, Akademicheskaya Str, 61108, Kharkov,Ukraine

E-mail: *voyev@kipt.kharkov.ua*

Trieste 20-24 April 2009 IAEA-ICTP Workshop

Theory and modeling-prediction behaviour on the basis terms of microstructural evolution

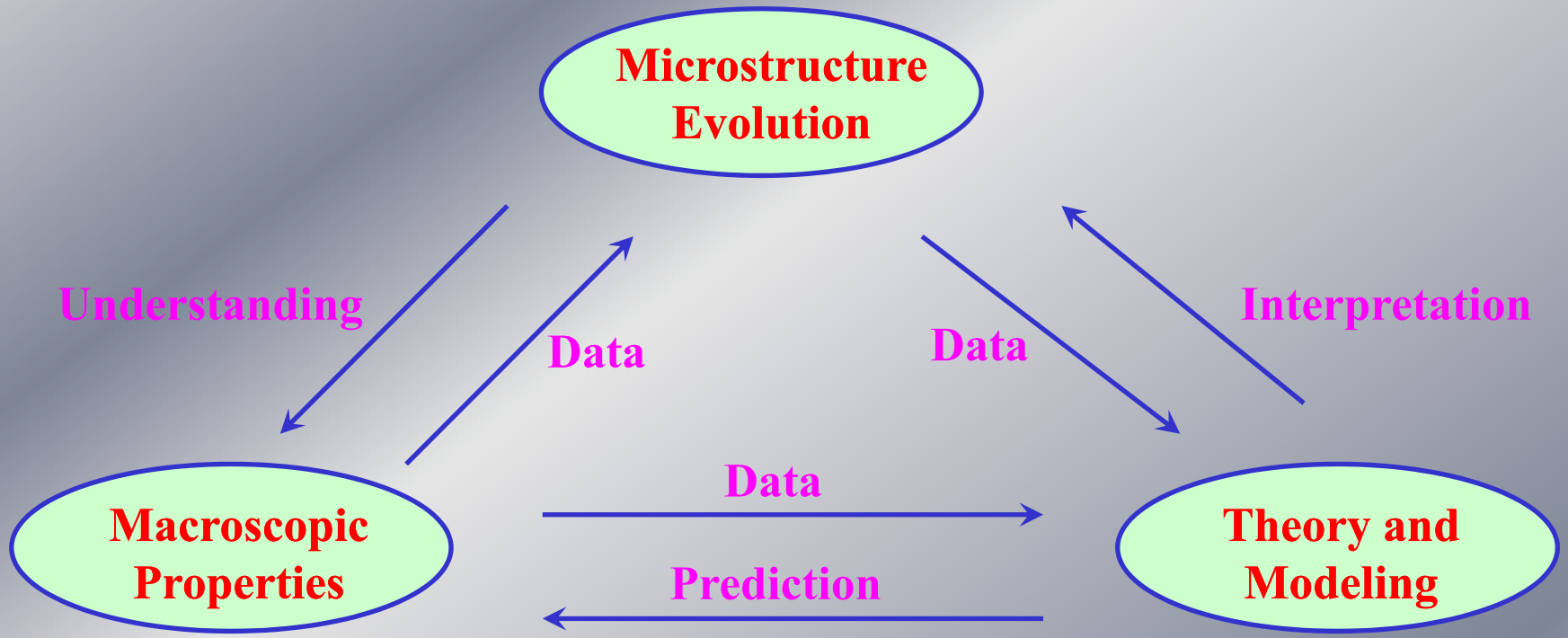

(D.Eyre, 1993)

Radiation damage and microstructure evolution

Because of the complexity of the material response to irradiation it is impossibly expensive to obtain data covering the wide range of conditions experienced in service. Extrapolation is therefore necessary and to do this with confidence requires an understanding of the physical mechanisms associated with the property changes.

Radiation damage is initiated at the atomic level, but the macroscopic effects that are the concern of the plant designer and operator arise from microstructural changes, such as the growth of voids, dislocation loops and precipitates. These microstructural changes can occur on a range of scales, from clusters of few atoms to features comparable to the grain size.

Reactors on thermal neutrons: WWER, PWR, BWR (power 440-1200 MW)

Mean density of thermal neutrons in core	$2.7 – 4.4 \cdot 10^{-13}$ n/cm^2 c	
Mean density of fast neutrons in core	$1.9\text{-}4.0 \cdot 10^{14}$	
Dose rate	10^{-7} dpa/s	
Temperature of coolant	on inlet	285 – 290 ^{0}C
	on outlet	320 – 325 ^{0}C
Density of fast neutrons flux on pressure vessel	$1 \cdot 10^{17}$ n/cm^2 s	
Fluence of fast neutrons (E.0,1 MeV) on pressure vessel during 40 years of operation	$\Phi t = 5 \cdot 10^{19} - 1 \cdot 10^{20}$ n/cm^2	
Dose rate for steel	10^{-10} dpa/s	
Dose of radiation damaging of pressure vessel during 40 years	0.1 dpa	

Materials of pressure vessels must guarantee the safe operation during service life.

Ferrite-pearlite, ferrite-martensite steels

Radiation damaging of pressure vessel steels

Primary formation of defects → nanostructure evolution → hardening → increase of temperature of brittle-ductile transition

Matrix defects: formation of clusters of point defects and of dislocation loops (1-10nm)

Formation of precipitates enriched by Cu and Mn - Ni, carbonitrides $(V, Cr)_7(C,N)_3$ (2-3 nm)

bcc→9R →3R →fcc

Segregation of phosphorus on grain boundaries and interphase boundaries.

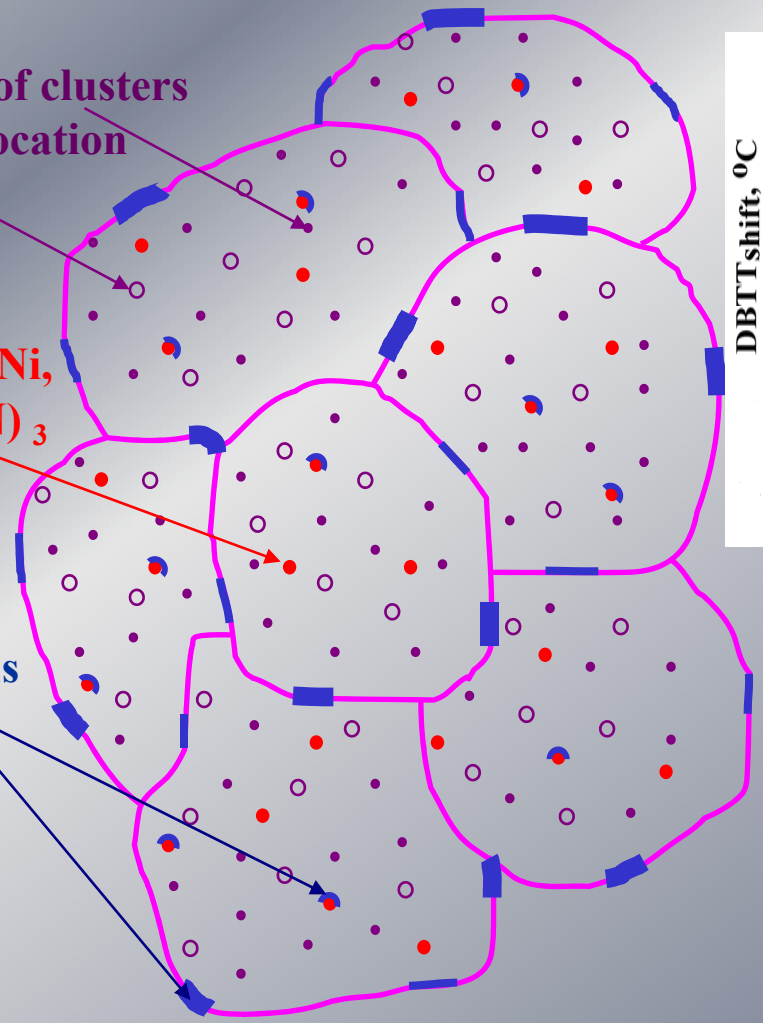

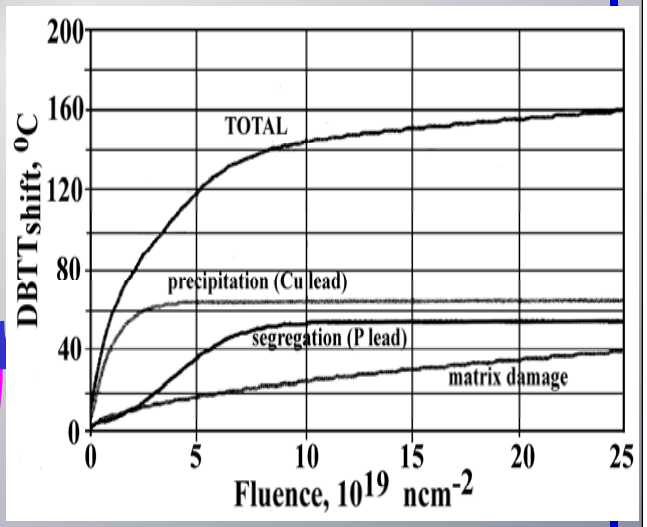

Radiation embrittlement:

$$\Delta T/T = AF^n$$

A – parameter depending of chemical composition of steels
n – exponent of power
F – fluence of fast neutrons

Dislocations behavior in A533 steel

A533 (Ni^+ 3MeV, D=1 dpa, T=290^{O}C)
Average diameter of loops d=2.5 nm , $\rho=10^{16}$ cm^{-3} [K.Fujii, 2004]

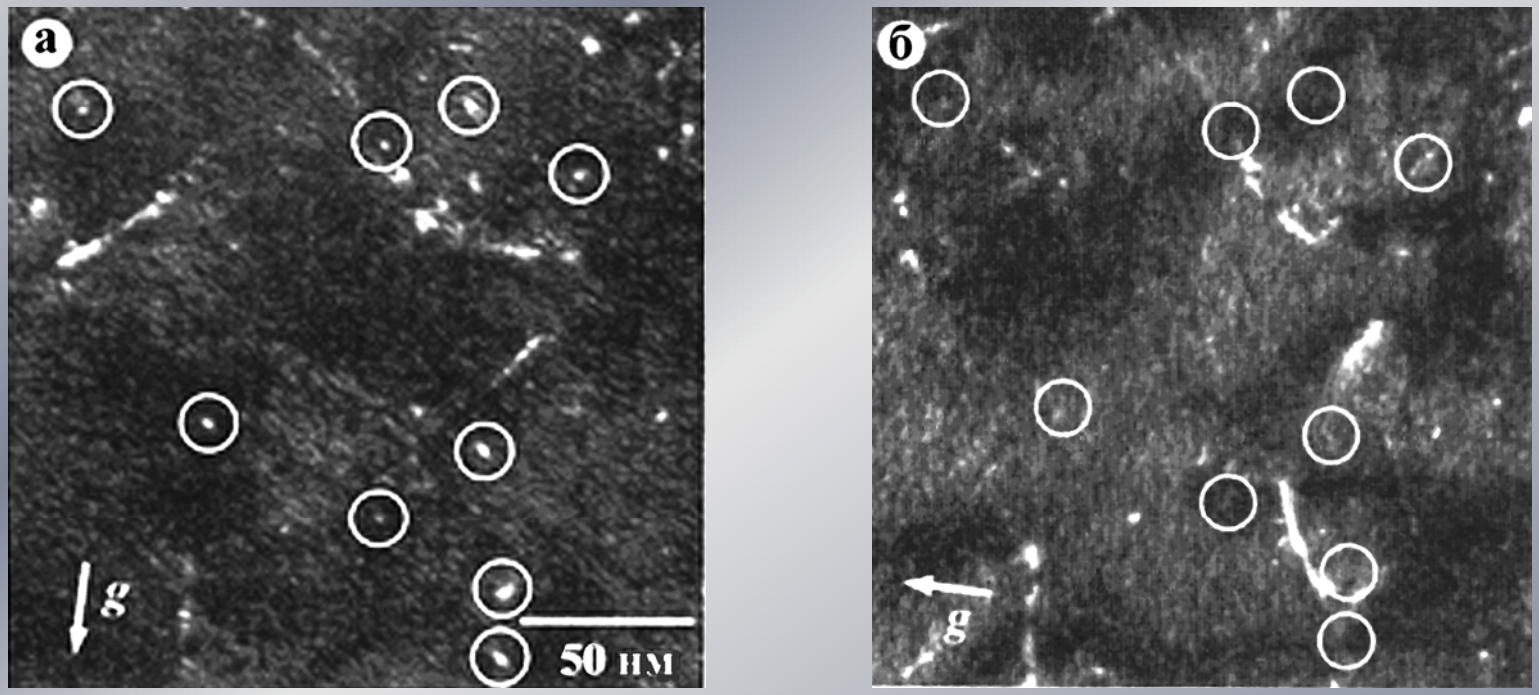

Dislocation loops images in different diffraction conditions : a) g = 020, b) g = 200.

Dislocation loops are visible as white dots. Absence of loops contrast on fig (b) means, that these dislocation loops have Burgers vector b = a<100>.

Evolution of microstructure of VVER-440 weld (0.012%P, 0.04%Cu)(B.Gurovich,1998)

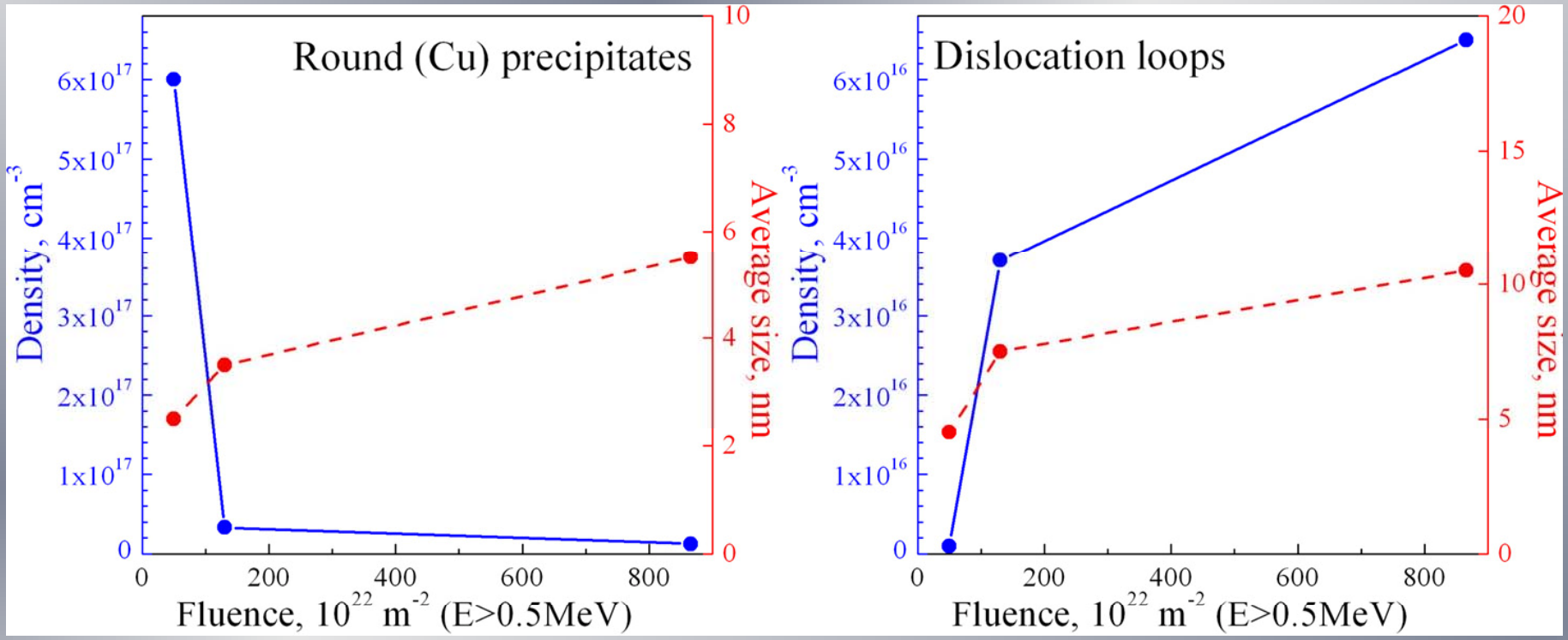

→ At low doses RE depends on Cu (*and P*)

→ Cu effect on RE has total saturation before $5 \cdot 10^{23}$ m^{-2}

→ At higher doses RE depends on dislocation loops (*and P*)

(B.Gurovich, S.Fedotova,2008)

MAIN RADIATION-INDUCED CHANGES IN VVER-1000 PRESSURE VESSEL STEELS (B.Gurovich,1999)

- Formation of dislocation loops and slow growth of their density in base and weld metals during operated limit of fast neutron fluence; their density increases by a factor of ~30–40 in weld metal beyond operated values of fast neutron fluence;
- Formation of rounded precipitates and increase of their density (Ni-Si-Mn – in weld metal and Ni-Si – in base metal) without saturation;
- Invariable density of disk-shaped precipitates (chromium carbides) in base metal (up to a fluence of ~1×10^{20} cm^{-2}) and some increase of carbides density with their average size decreasing with further fluence growth;
- Absence of radiation-induced disk-shaped precipitates in weld metal;
- Formation of intergranular impurities segregation (phosphorous first of all).

Some aspects of the precipitates transformation processes

9R → 3R → FCC

- *Detwinning of 9R precipitates*
- *Rotation (009)of 9R planes*
- *Removal of regular stacking faults from (009) base planes*
- *Transformation into FCC structure*

Twinning 9R copper precipitation in alloy Fe-Cu

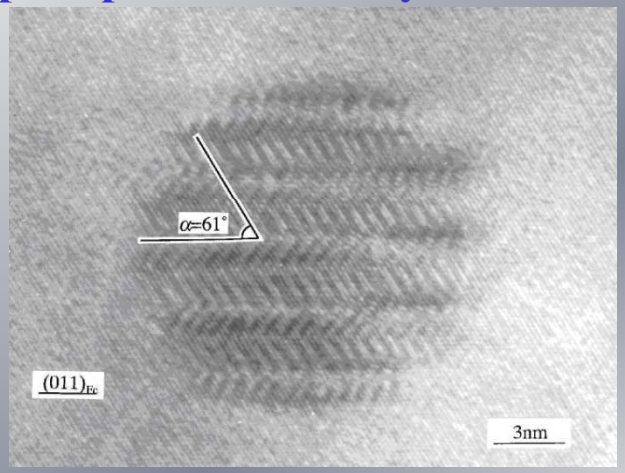

Structure of upper part -9R, and low part 3R

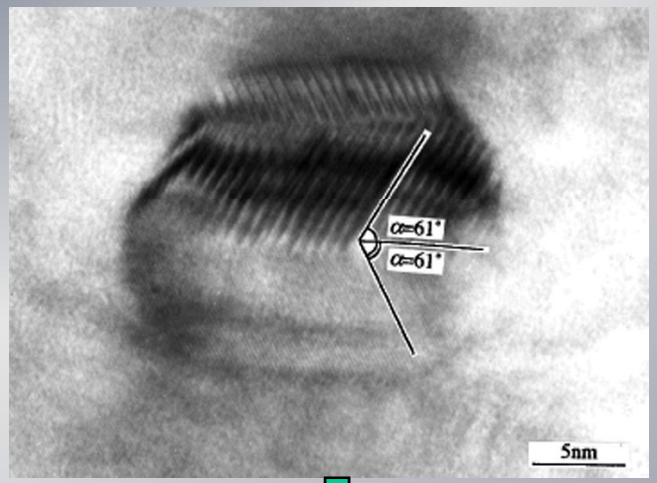

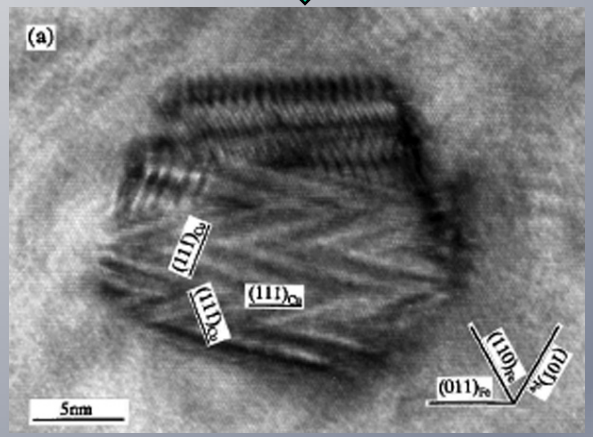

Precipitates with intermediate between 3R and FCC structure.

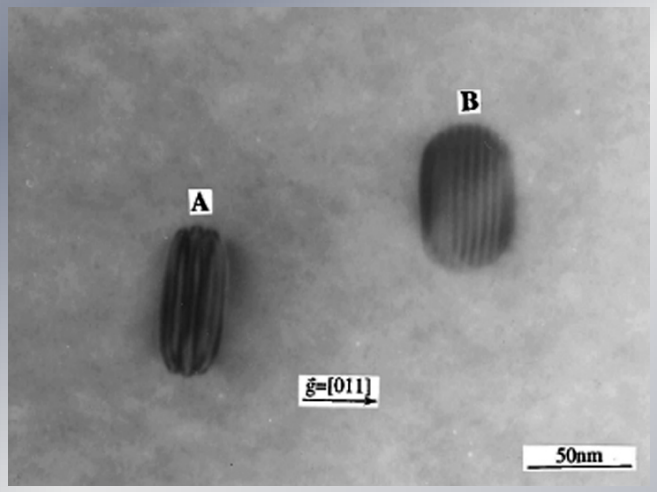

Precipitates with FCC and FCT structure.

Vacancies, intersticials, transmutations, etc. (L.Debarberis,2007)

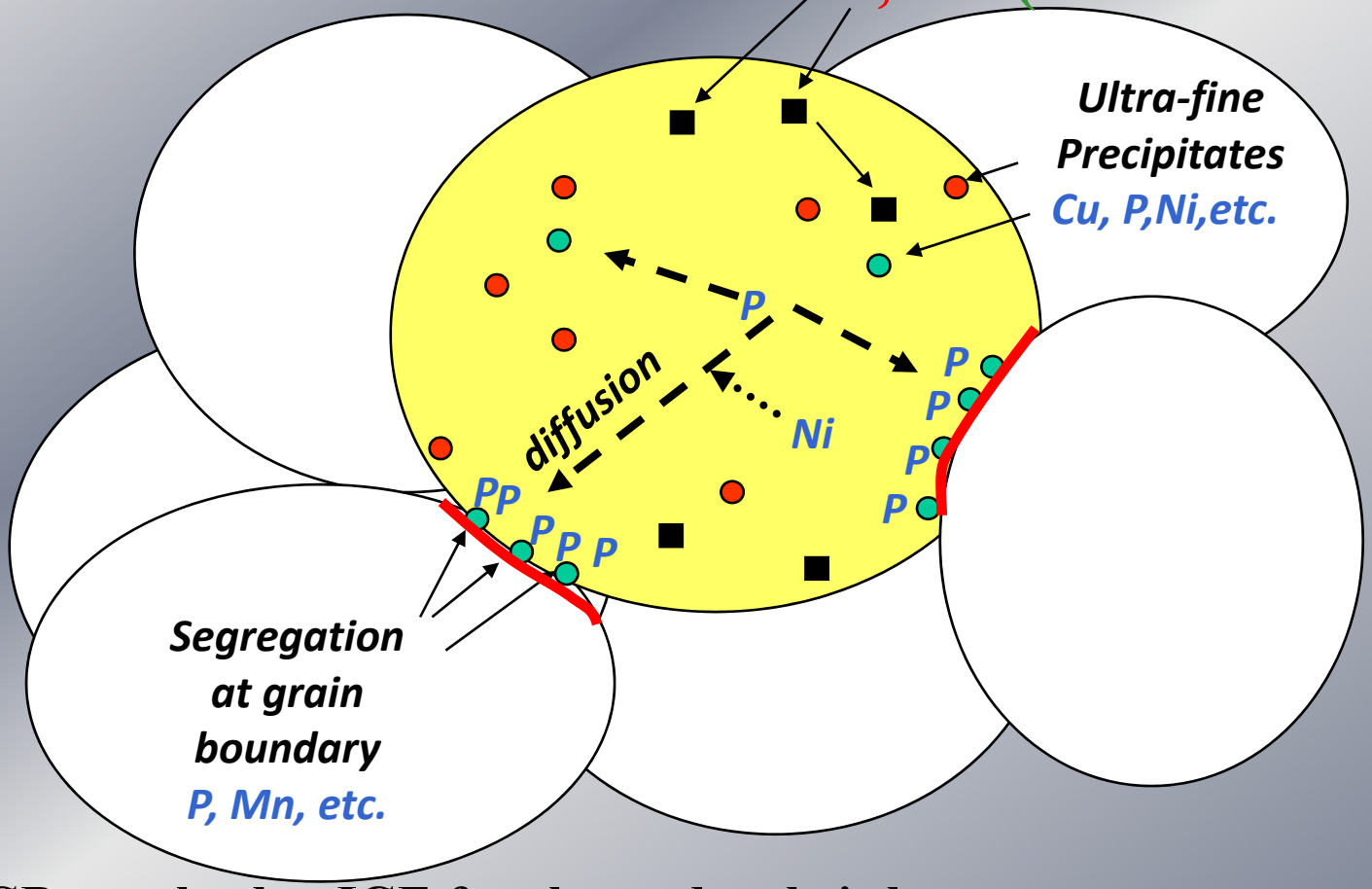

- P to GB may lead to IGF & enhanced embrittlement
- Need to predict P segregation under irradiation
- Need of reliable indicator for non-hardening embrittlement
- Reduce uncertainties on RPV properties (EOL)

Features of radiation stimulated phosporous segregation in vessel steels (Yu. Nikolayev, 2001)

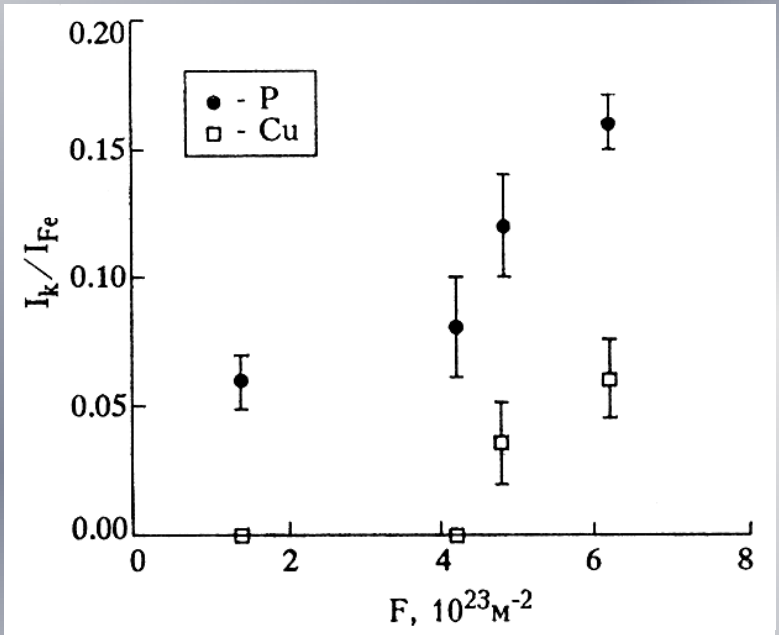

Change of intensity of Auger-peaks of phosphorus (120eV) and copper (920eV) in relation to intensity of Auger-peak of iron (703eV) on boundaries of grains as function of fast fluence neutrons.

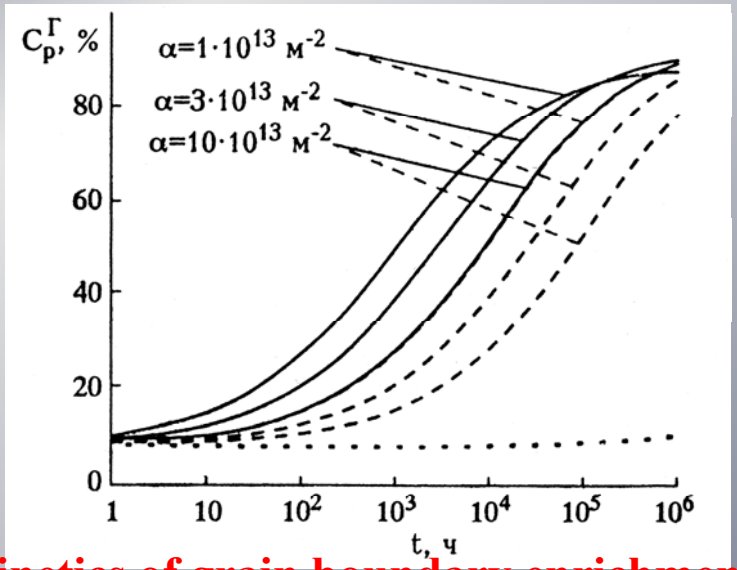

Kinetics of grain boundary enrichments by phosphorus in steel with 0,02 % P and 1 % N (T=300°C).
Without an irradiation (a dot line),
10^{-8} dpa/s (a solid line),
10^{-9} dpa/s (a dash line),
a – dislocation density.

Analysis of WWER-440 and PWR RPV welds surveillance data to compare irradiation damage evolution, L. Debarberis et al., Journal of Nuclear Materials, Volume 350, 2006

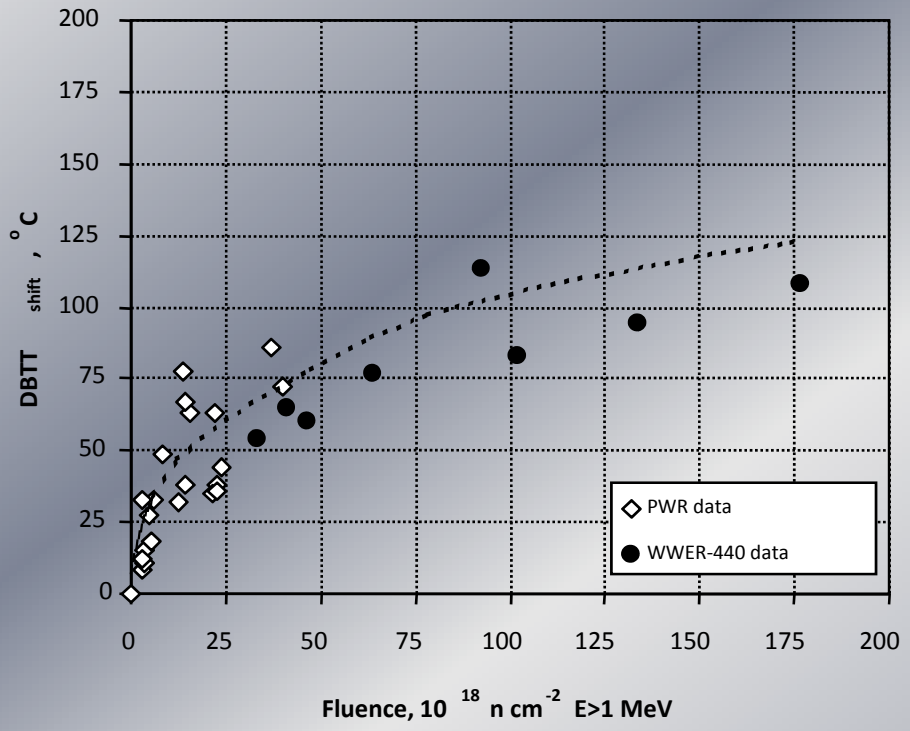

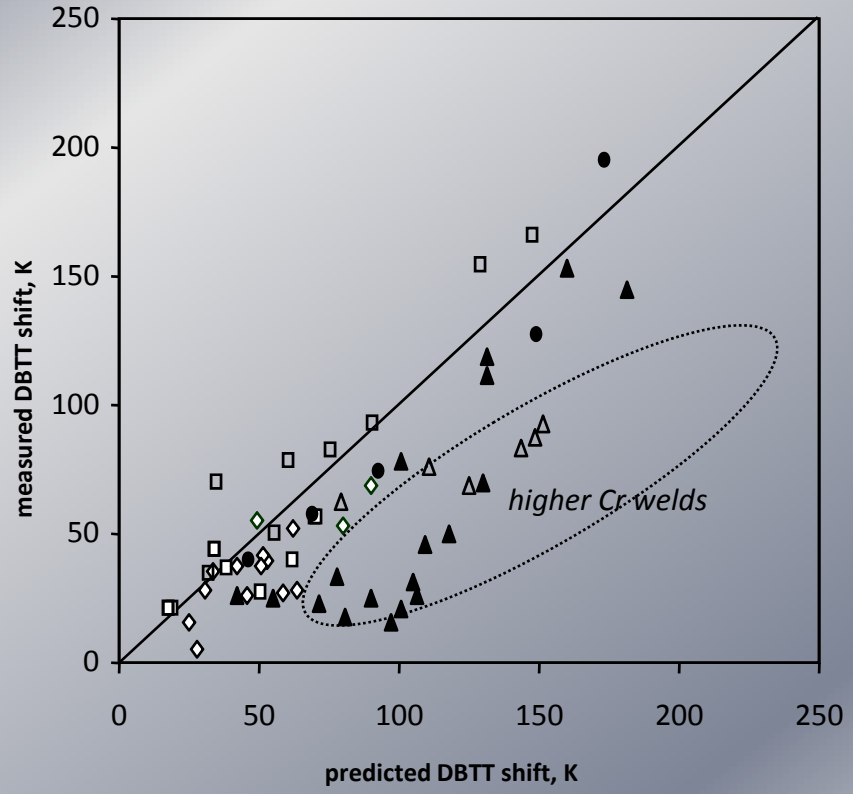

Evidence for Chromium stabilisation of irradiation damage in RPV weld metals
L. Debarberis, H. Hein, International Journal of Pressure vessel and Piping, 2006

Indexes of some planes and directions in HCP lattice

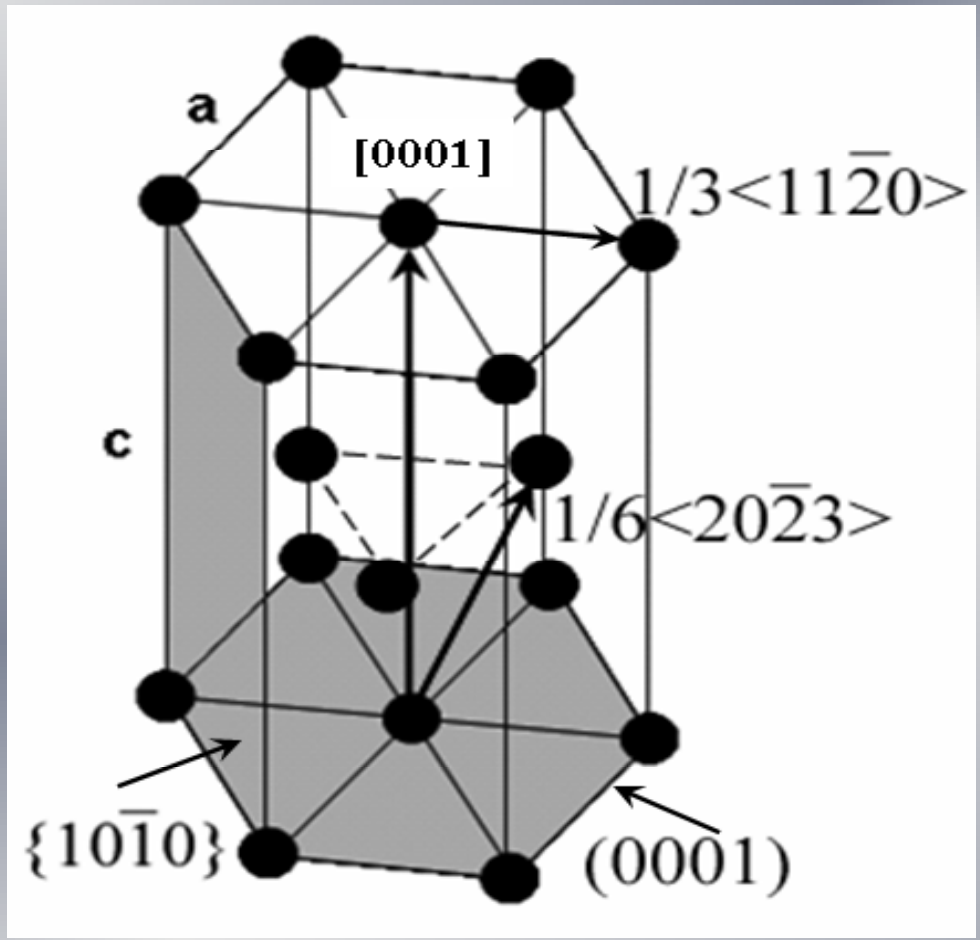

Dislocation loops in HCP crystals nucleated on prismatic {1010}, basic (001) and pyramidal {1011} planes have Burgers vectors (1/3)<1120>, (1/6)<2023> or (1/2)[0001] and (1/3)<1123> respectively.

σ defect production by thermal neutrons	σ defect production by fast neutrons
Zr – 0,3 barn	860 barn
Ni – 26.2 barn	850 barn
Cr – 20.8 barn	948 barn
Fe – 12.1 barn	844 barn

Microstructure of E110 alloy (irradiation at T=300^{0}C, D≈30 dpa, BOR-60)

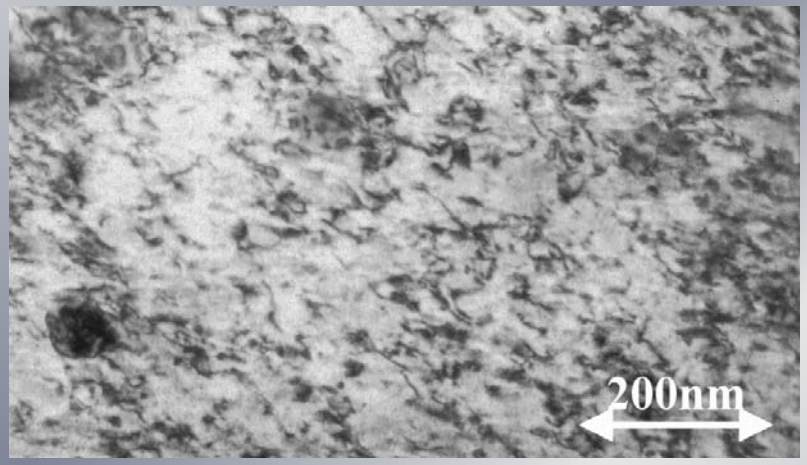

Loops and dislocations of <a>-type

Density of <a> loops ~3*10^{15}cm^{-3}, average size ~10nm,
density of dislocation net <a>-type ~3*10^{10}cm^{-2}.

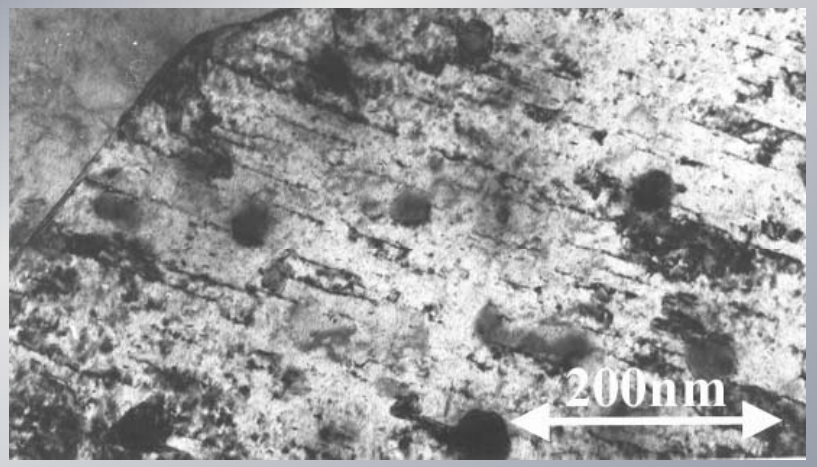

Dislocations of<c>-type

Density of <c> dislocation about ~3.5*10^{10}cm^{-2}

Microstructure of E635 alloy (irradiation at T=300^{0}C, to D≈25 dpa, BOR-60)

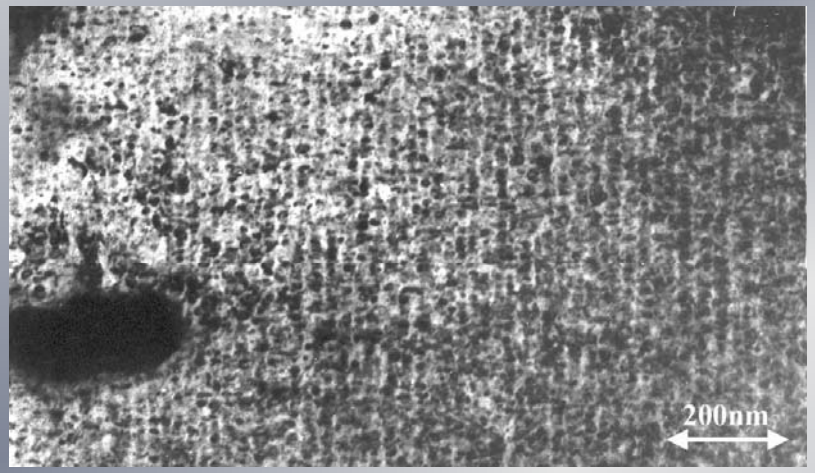

Alignment of dislocation loops <a> -type,

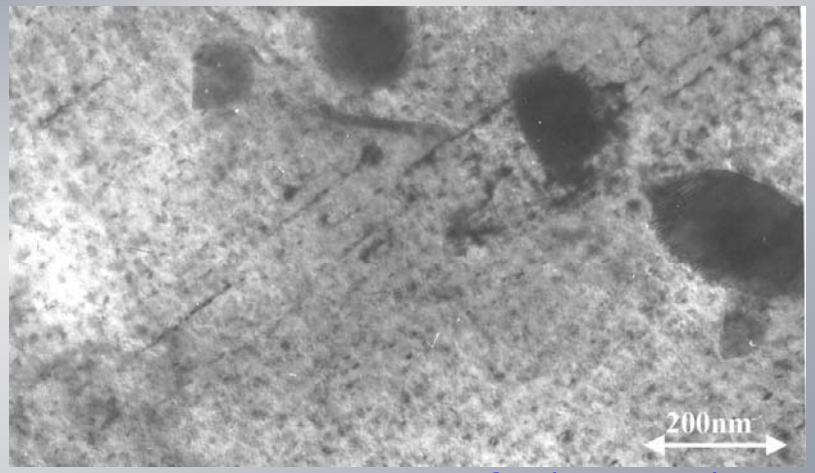

<c> -component of dislocation structure

Average size of dislocation loops <a> -type ~ 12 nm, and concentration $6*10^{15}cm^{-3}$. Alignment of dislocation loops in the plane {0001} are observed. Concentration of <c> -component of dislocation loops is about ~ $6*10^{14}cm^{-3}$. In the E635 alloy take place phase transition $(Zr,Nb)_3Fe \rightarrow \beta$-Zr

Major structural characteristics of irradiated and unirradiated E635 alloy

Dose, dpa	Precipitate							Dislocation loops	
	Diameter μm	Concentration 10^{20}м$^{-3}$	Type	Content, at%				Type	density, 10^{14}м$^{-2}$
				Zr	Nb	Sn	Fe		
0	0.12	5.0	$Zr(Nb,Fe)_2$	37	3	0.1-1.0	26	a	0.2
								c	0.1
59	0.01	500	Plate (non coherent)					a	34
	0,132	0,15	β-Nb BCC a=0,346nm	46-66	32-53	<0,9	0,3-10,5	c	3,5
			α-Zr (matrix)	98		0,8-1,3	0,45-0,60		

Comparison between structural characteristics of irradiated E110 and E635 alloys

After irradiation at 300^0C to 30 dpa (BOR-60) microstructure evolution of E110 and E635 zirconium alloys have next features:

1.Density of <c> type dislocation in the E110 alloy increase more rapidly then in the E635 alloy.

2. In the E635 alloy was observed alignment of dislocation loops <a> type in the rows.

3. In the E635 alloy take place phase transition
$(Zr,Nb)_3Fe \rightarrow \beta$-Zr

4. In the E635 alloy was observed precipitation of particles irradiation-induced finely-dispersed coherent precipitates.

Microstructure of Zircaloy alloys (M.Griffits, 1988)

unirradiated alloy

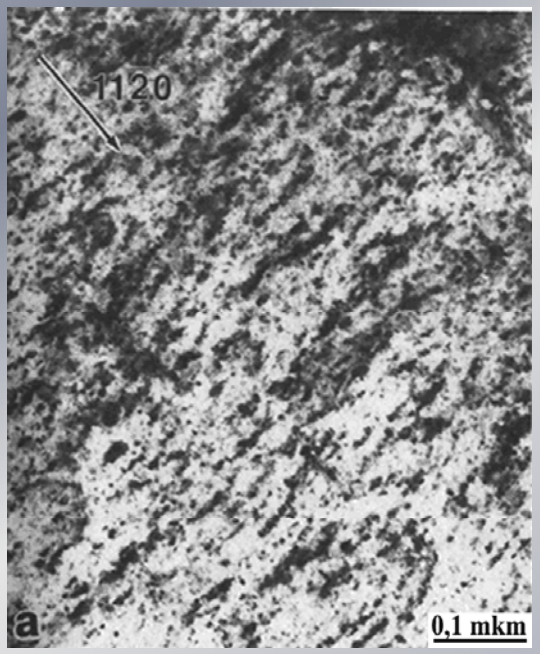

Zy-2,D=3сна,T=77°C

Dislocations loops of <a>-type

Density of <a> loops ~$2*10^{20}m^{-3}$, average size ~5nm,

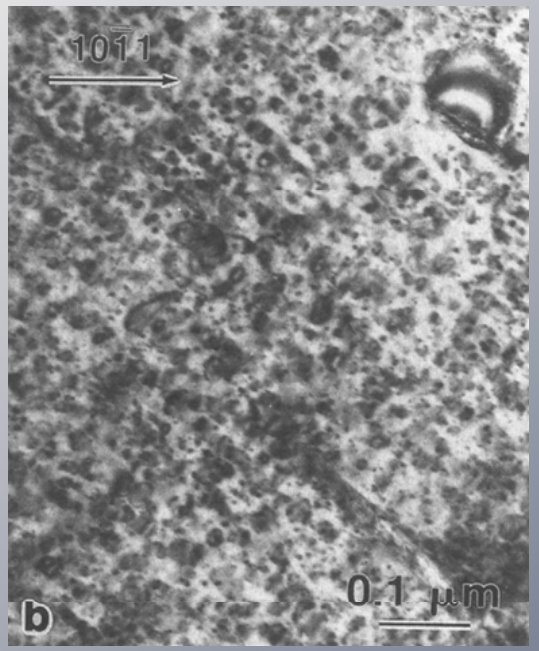

Zy-4, D=0.5сна,T=307°C

Dislocations loops of <a>-type

Density of <a> loops ~$2.6*10^{22}m^{-3}$, average size ~15nm,

Amorphisation of precipitates Zr $(Cr, Fe)_2$ in zircalloy – 4, T=200°C

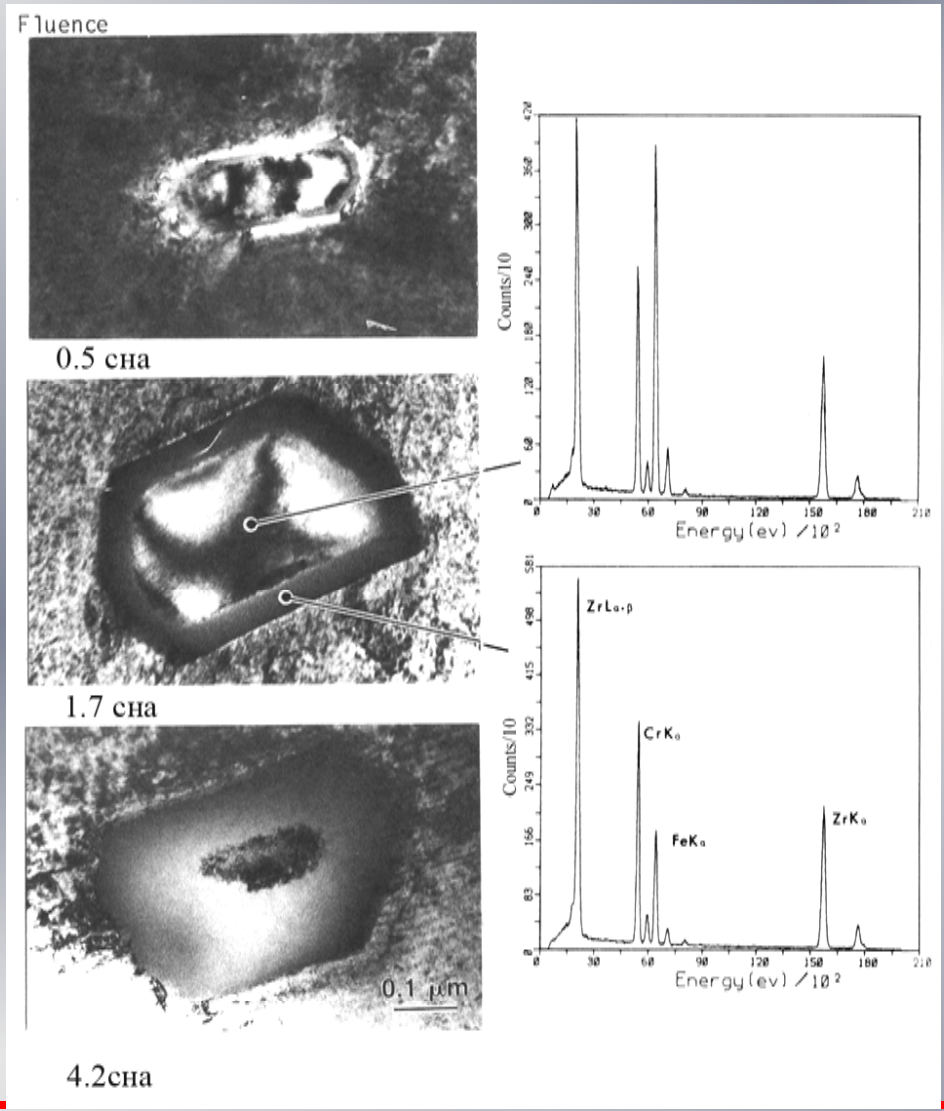

At irradiation temperature 280-310° C precipitates Zr $(Ni, Fe)_2$ remain crystallic while precipitates Zr $(Cr, Fe)_2$ became amorphous

Dissolution of Zr$(Cr, Fe)_2$ particles with a high concentration of Cr-rich precipitates surrounding this particles, may be related to the fact that Cr is a much slower diffusing species in the Zr matrix compared with Fe and Ni.

The main products of nuclear transmutation in Zr-based alloys in reactor VVER-1000 during 72 month (in appm)

Alloy	H	He	Sr	Co	Y	Mo	K (from Ca)	Ag, Cd, In
Zr – 2	6,037	4,377	4,274	0,149	0,310	148		$6 \cdot 10^{-3}$
Zr – 4	4,866	4,314	4,272	0,04	0,310	148		$6 \cdot 10^{-3}$
Zr – 1%Nb	4,540	4,506	4,312		0,492	152		
Zr – 2,5%Nb	4,818	4,732	4,247		0,765	157		
635	5,04÷ 5,294	4,47÷ 4,483	4,25÷ 4,229	0,03÷ 0,048	0,55÷ 0,51	152÷ 153	0,643	$(4 \div 6) \cdot 10^{-3}$

Pressure Tube Operating Conditions in Candu reactors

- temperature: ~250 - 310°C
- stress: 130 MPa hoop & 65 MPa axial
- fast neutron flux: 3.5×10^{17} $n \cdot m^{-2} \cdot s^{-1}$, E>1MeV, peak reactor centre

each atom displaced ~1.5 times per year

Radiation Damage in Irradiated Zr-2.5Nb Pressure Tubing (300°C), $\phi = 2x10^{13} n \cdot cm^{-2} \cdot s^{-1}$ (M.Griffits, 2007)

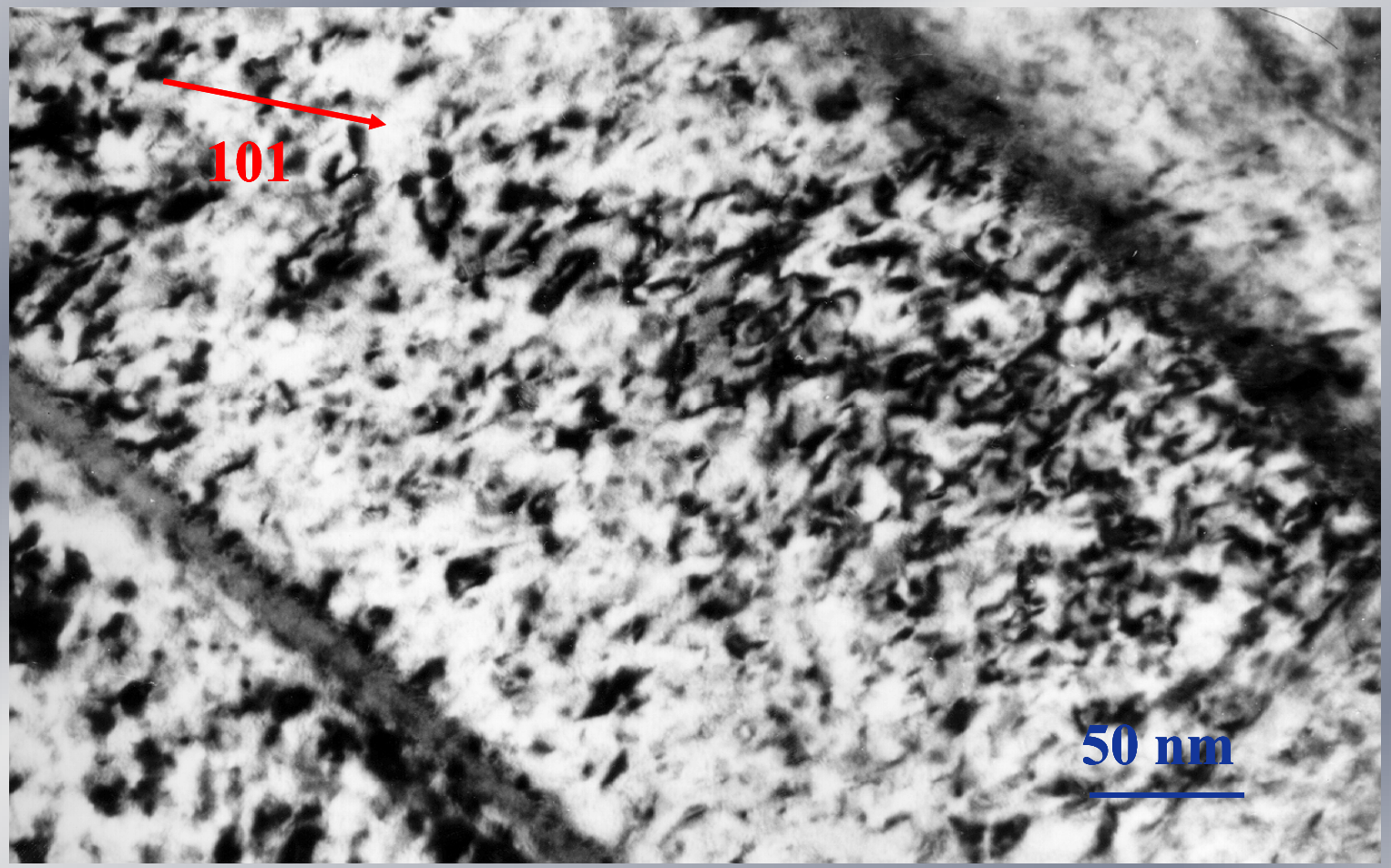

Beta-Phase State in Zr-2.5Nb Pressure Tubes in Reactor Candu (M.Griffits, 2007)

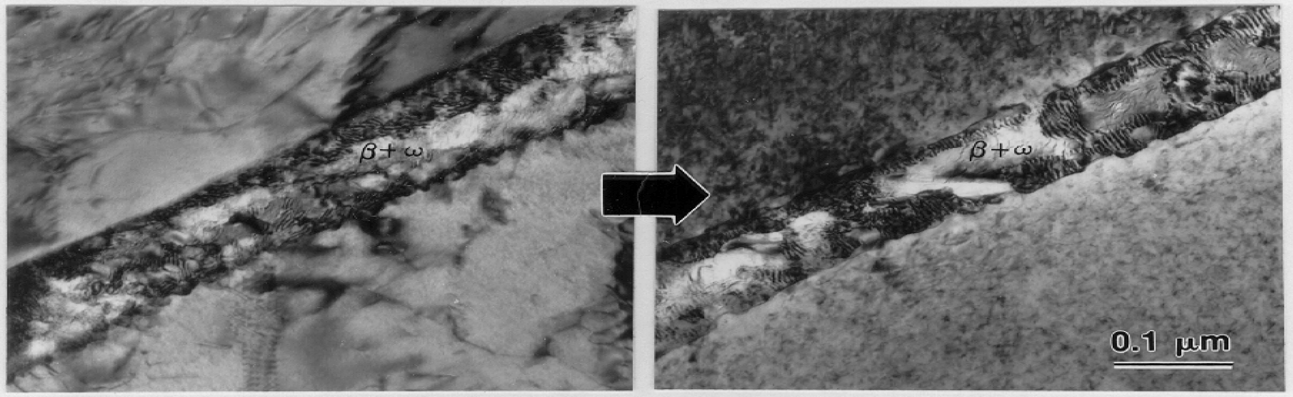

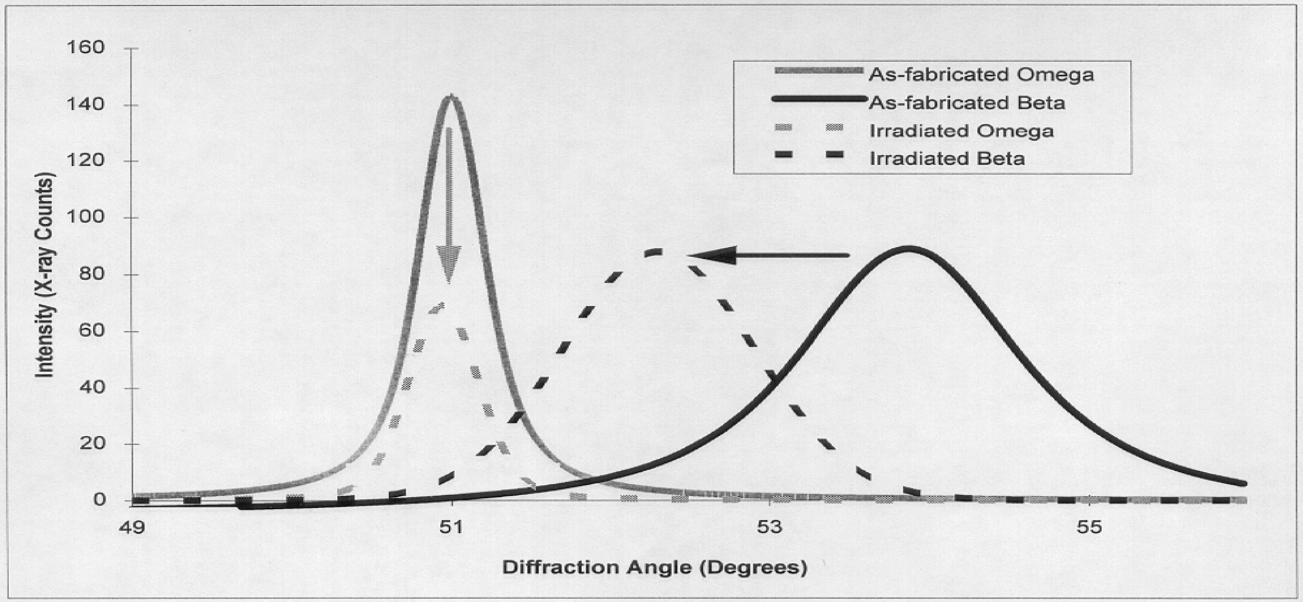

Dislocation Structure (M.Griffits, 2007)

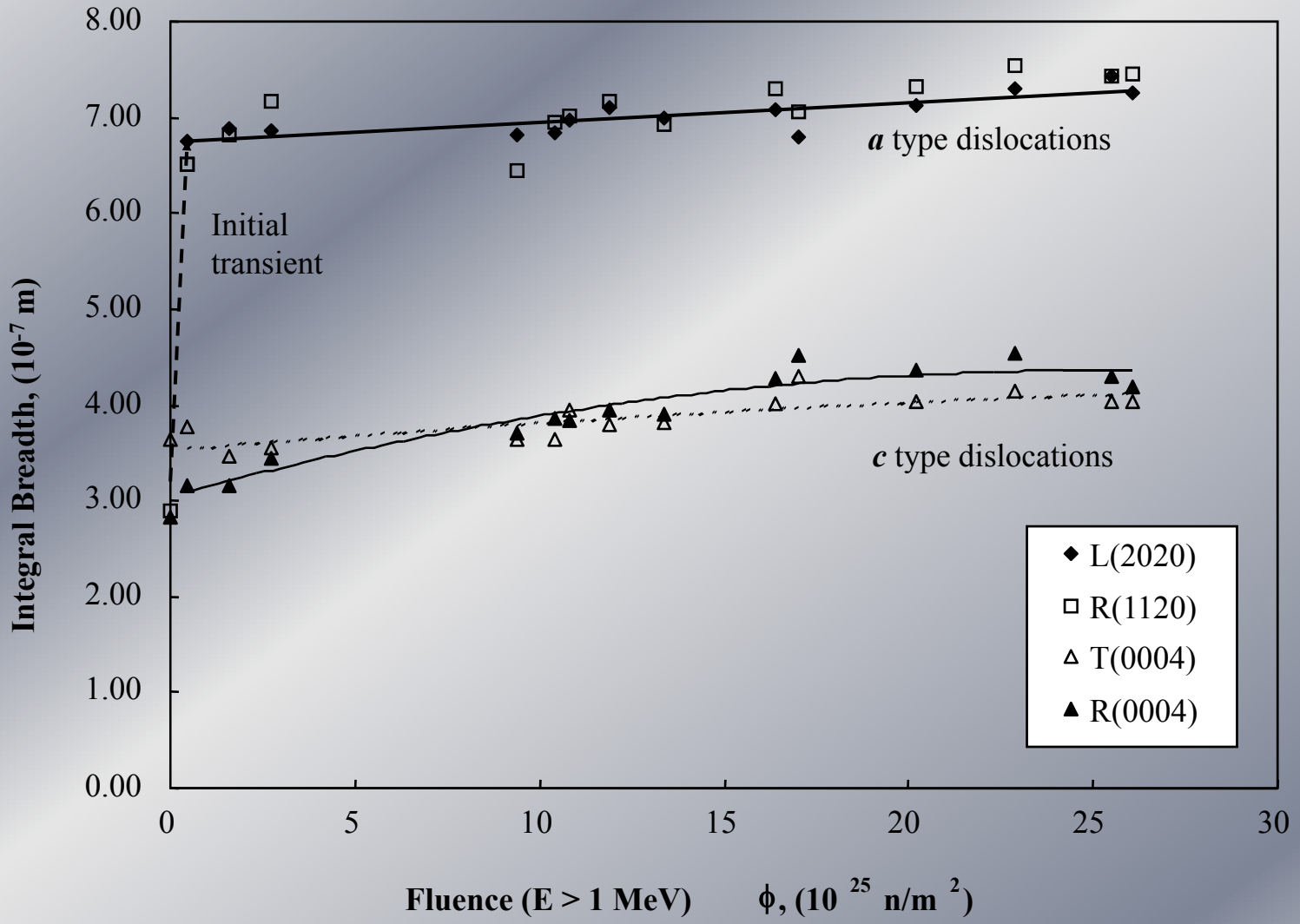

Reactors on fast neutrons-nuclear fuel breeding, annihilation of long-lived isotopes

Density of neutron flux	$3 \cdot 10^{15} - 10^{16}$ n/cm^{2}s
Rate of He generation	20 – 30 appm/year
Dose rate	100 – 200 dpa/year
Temperature	400 – 650^{0}C

The main phenomenon limiting the achievement of high burn-up of nuclear fuel is the radiation swelling of cladding and wrappers of fuel elements (FE).

✓ Cladding of FE –austenitic steels:
18Cr10NiTi→ EI-847(16Cr15Ni3MoNb) → EP-172(16Cr15Ni3MoNbB) →
ChS-68(16Cr15Ni2Mo2MnTiVB) → EK-99(15Cr15Ni3MoTi+REE,Sc)→
EK-164 (16Cr19Ni2Mo2MnVNbTiB) →
PNC 316 (Ni- 13.8; Cr- 16.5; C- 2.5; Ti-0.098; Nb- 0.07; Si- 0.93; P-0.031; Mn-1.78;B- 0.0044)

✓ Wrappers of FE- austenitic → ferritic-martensitic steels
18Cr10NiTi(BN-350) → EP-450(12Cr1MoNbVB(BN-600) →
EP-823(12CrMoWSi(BREST)

Main relations in structure and composition of SS under irradiation

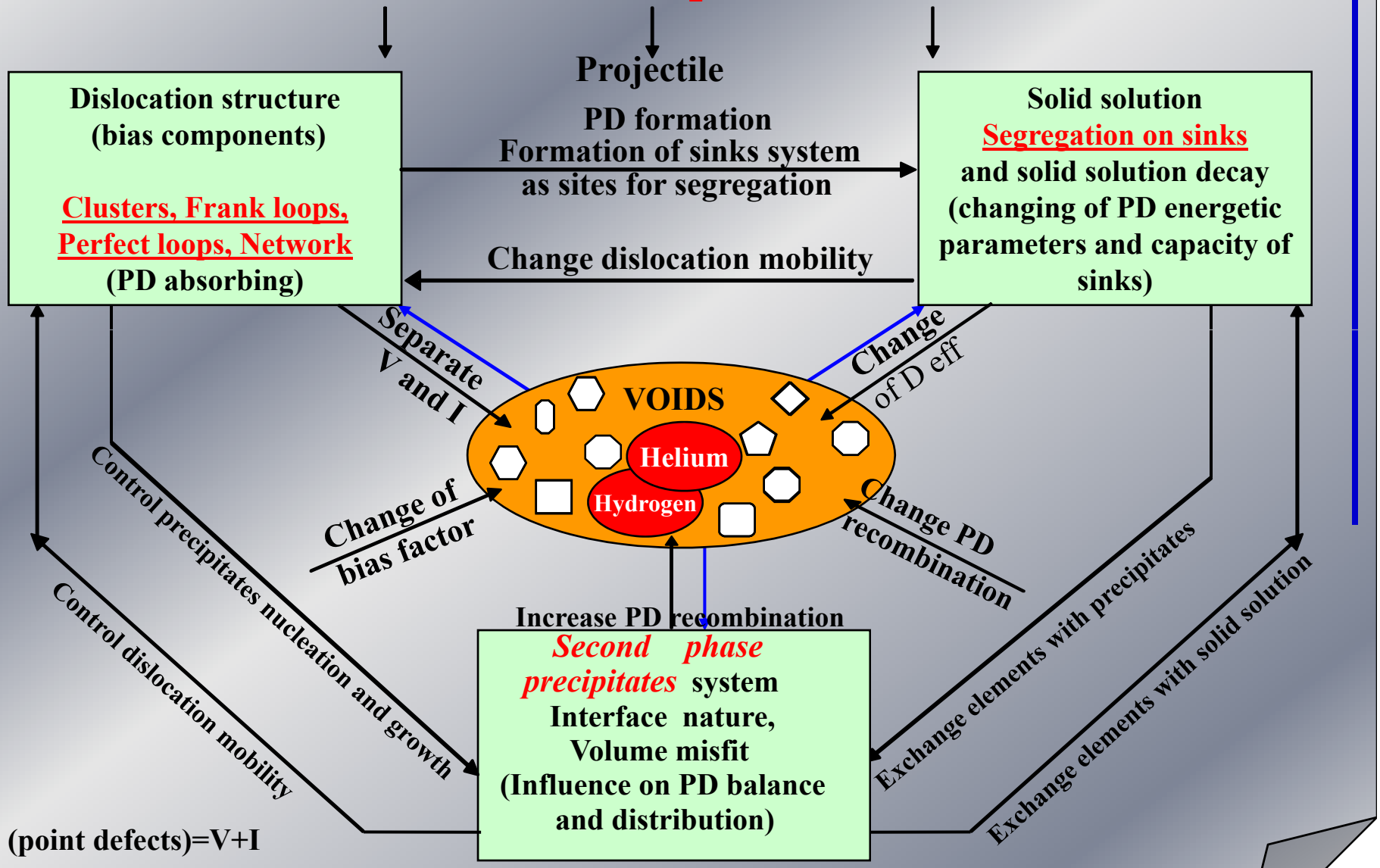

Stages of dislocation structure evolution in irradiated steel EI-847 (Cr^{3+}, E=3 MeV, $T_{ir.}$=650°C, K=10^{-3}dpa/s), a) D=0.5 dpa, b) D=2 dpa, c) D=10 dpa, d) 15 dpa, e) D=25 dpa.

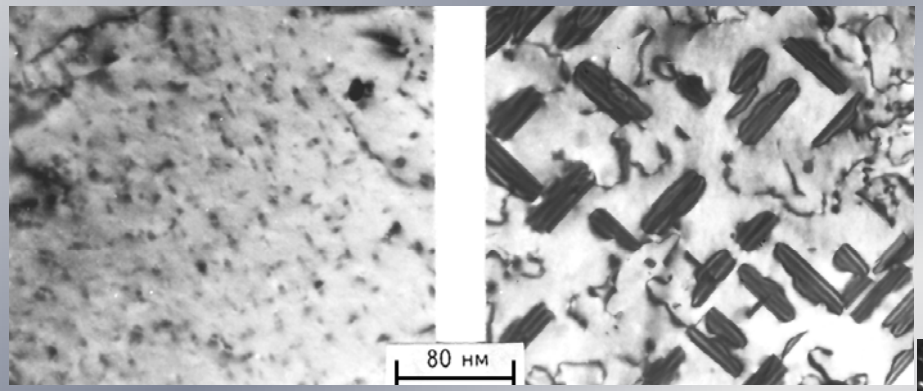

$$a/3\langle 111\rangle + a/6\langle 112\rangle = a/2\langle 110\rangle$$

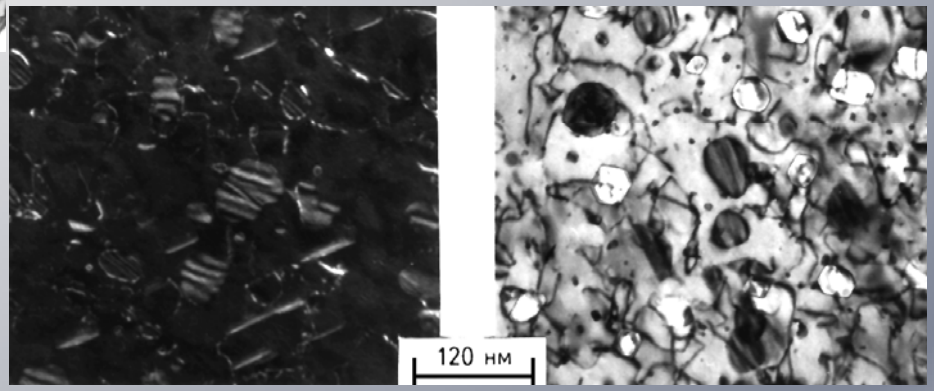

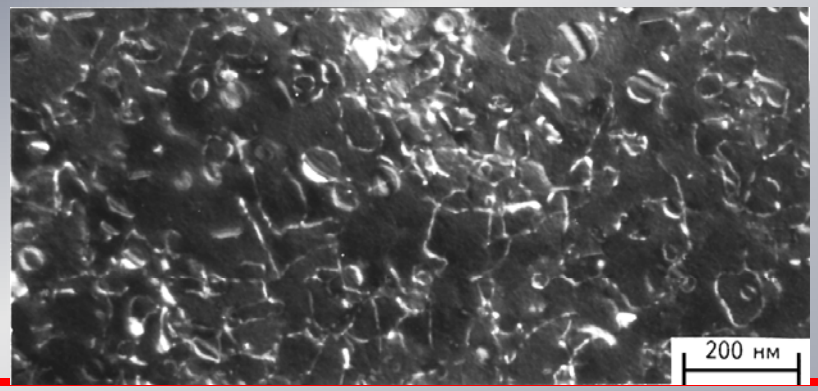

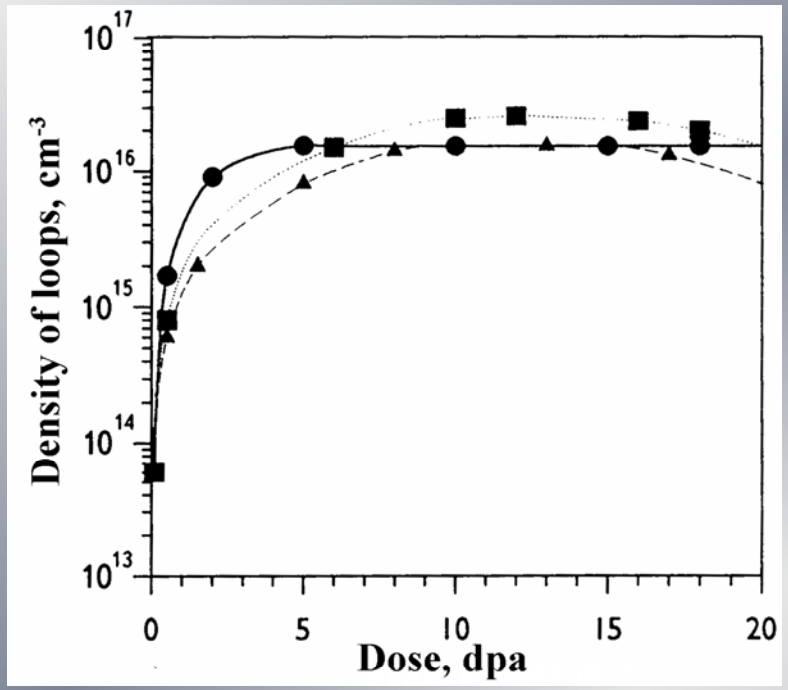

Dose dependence of the density of defected dislocation loops ($T_{irr.}$=625°C): ▲ - EI-847 (SA) (Cr^{3+}, E=3 MeV); ● - AISI 316 (SA) (n, EBR-II); ■ - EI-847 (SA) (Cr^{3+}, E=3MeV, 20 appm He)

Variation of the density of dislocations with the dose in materials with different structure state:
● - EI-847 (SA), ○ - EI-847 + 30% CW (Cr^{3+}, E=3MeV, $T_{irr.}$=500°C); ■ - EI-847(A), □ - 847+30%CW (Cr^{3+}, E=3MeV, $T_{irr.}$=600°C)

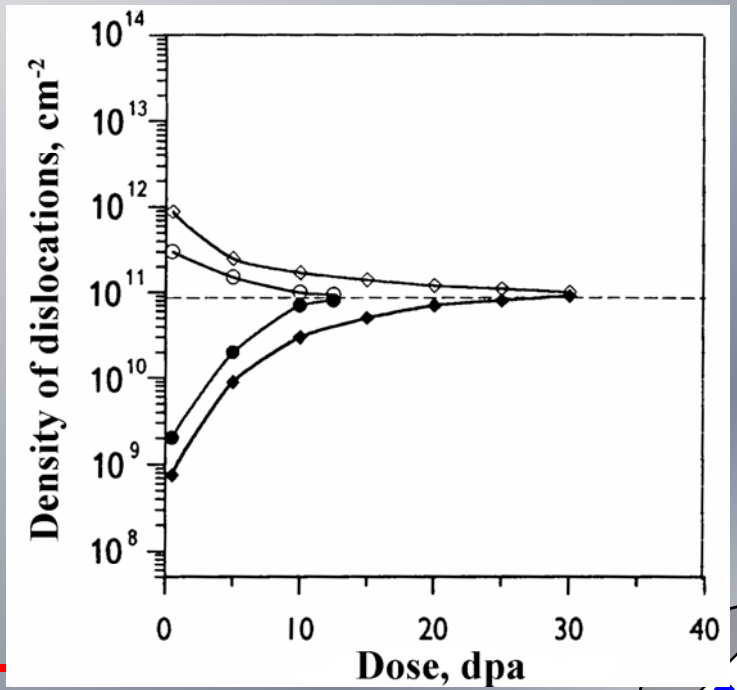

Characteristics of Frenkel loops in dependence on the ratio He/dpa (steel Fe-15Cr-20Ni, D= 3 dpa)(H.Takahashi,1997)

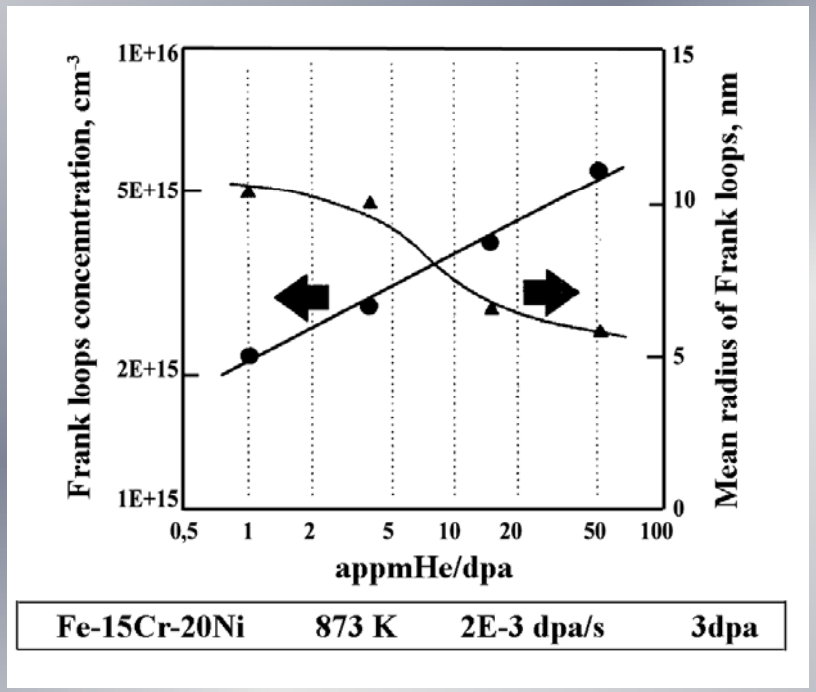

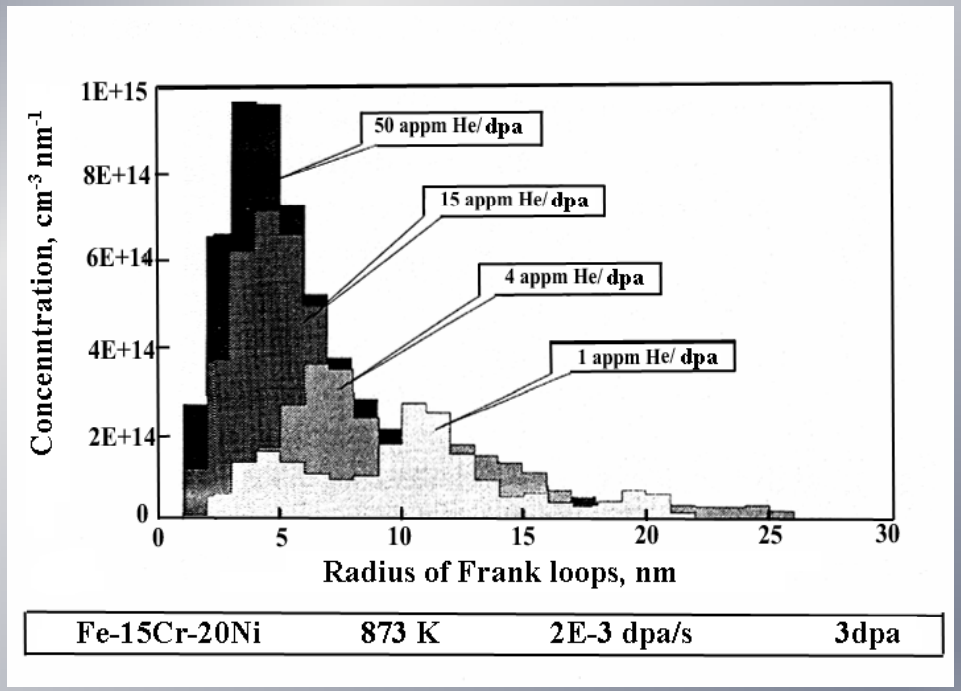

Evolution of dislocation structure in F/M steel EP-450 (Cr^{3+}, E= 3 MeV, $T_{irr.}$= 500°C) a) D = 0.1 dpa; (dark field image), b) D=0.5 dpa; c) D=5 dpa; d) D=15 dpa (dark field image)

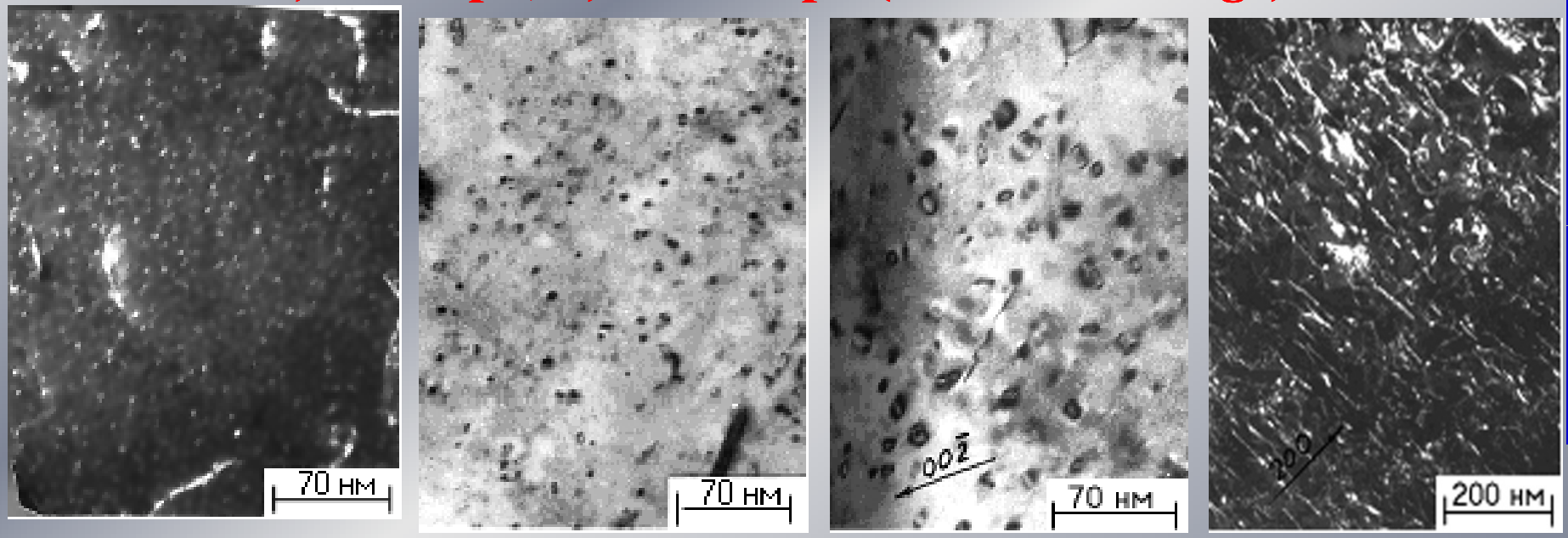

15 dpa Fe-3%Cr a<100>

Fe-9%Cr a<100>, a/2<111>

Fe-12%Cr a<100>, few a/2<111>

Fe-18%Cr few a<100>, a/2<111> (D. Gelles, 1986)

Distribution of the elements near the stationary boundary in steel EI-847 (BOR-60, E>0.1 MeV, D=30 dpa, T_{irr}=540°C)

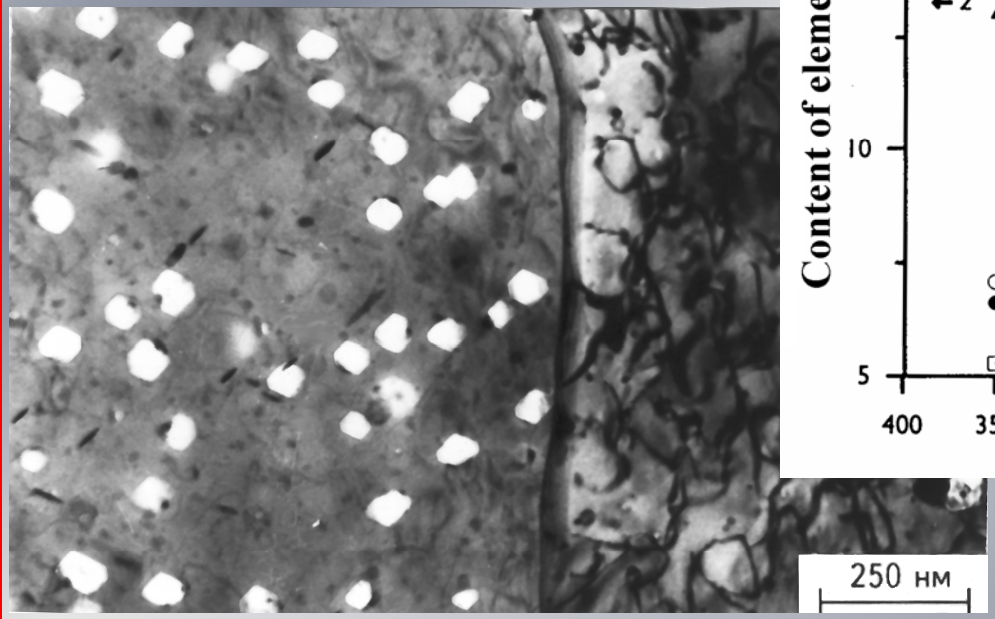

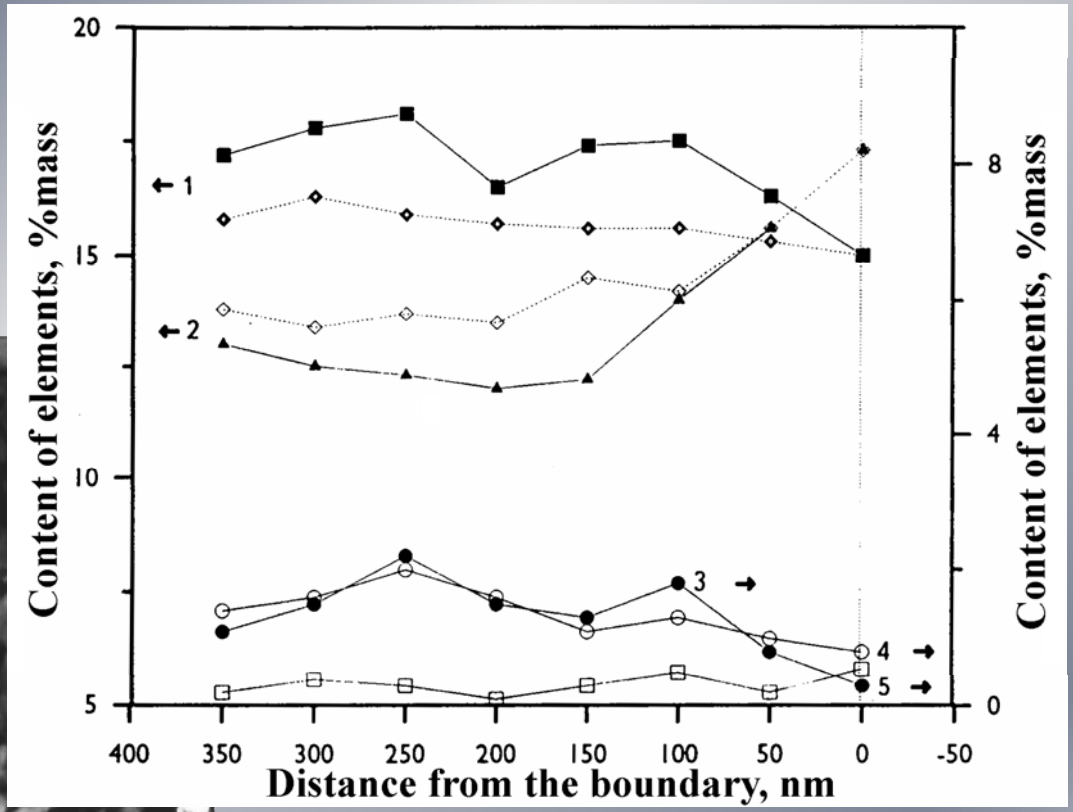

1 - Cr, 2 - Ni, 3 - Mo, 4 -Nb, 5 - Si

Influence of He on the segregation of solute elements on the grain boundary in steel 316 (e^-, E= 1 MeV, $T_{irr.}$ = 720 K, D=15 dpa) 1 - Cr, 2 – Ni (--- without He, ----- - 1000 appm He) (H. Takahashi, 1997)

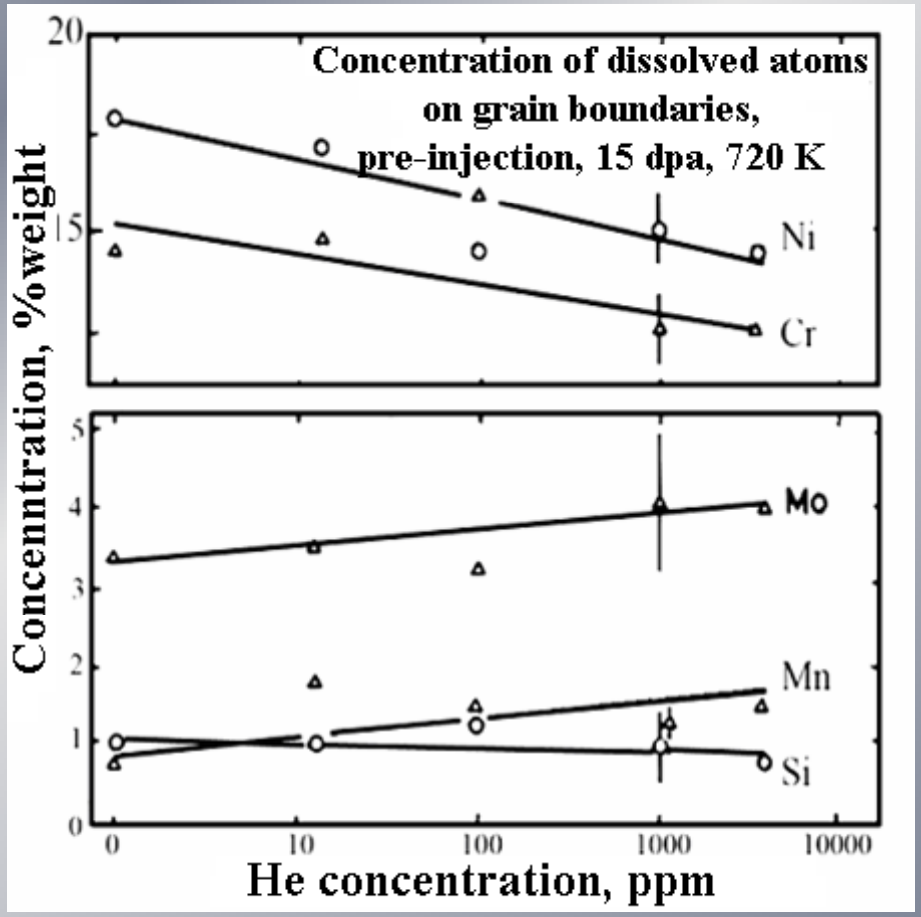

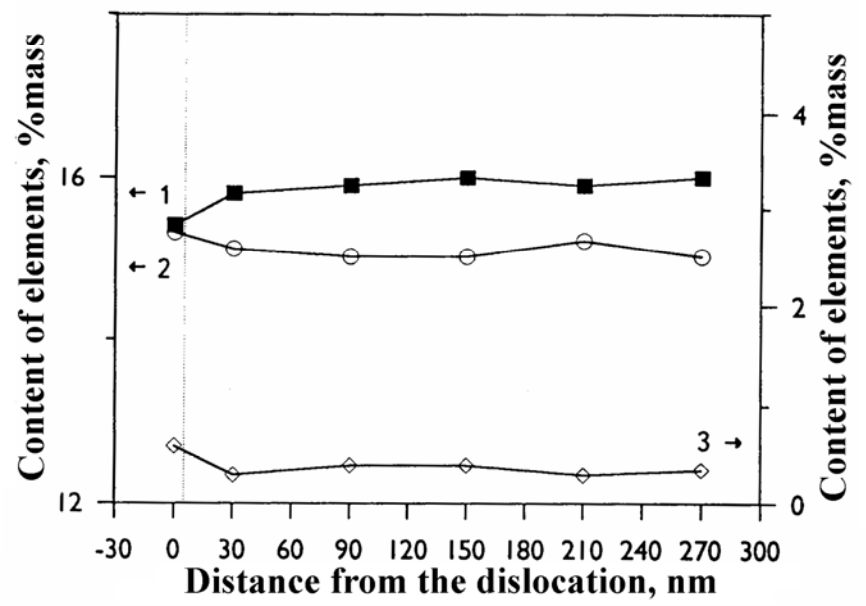

Segregation profile of dislocation segment (1-Cr, 2-Ni, 3-Si) (EI-847, Cr^{3+}, E=3 MeV, $T_{irr.}$=600°C, D=45 dpa)

Elements Distribution in the plane of stacking fault of Frank loop (dotted lines show the mean content of elements in matrix): 1 – Cr, 2-Ni, 3-Si (EI-847 (SA), (Cr^{3+}, E=3 MeV, $T_{irr.}$= 600°C, D=25 dpa)

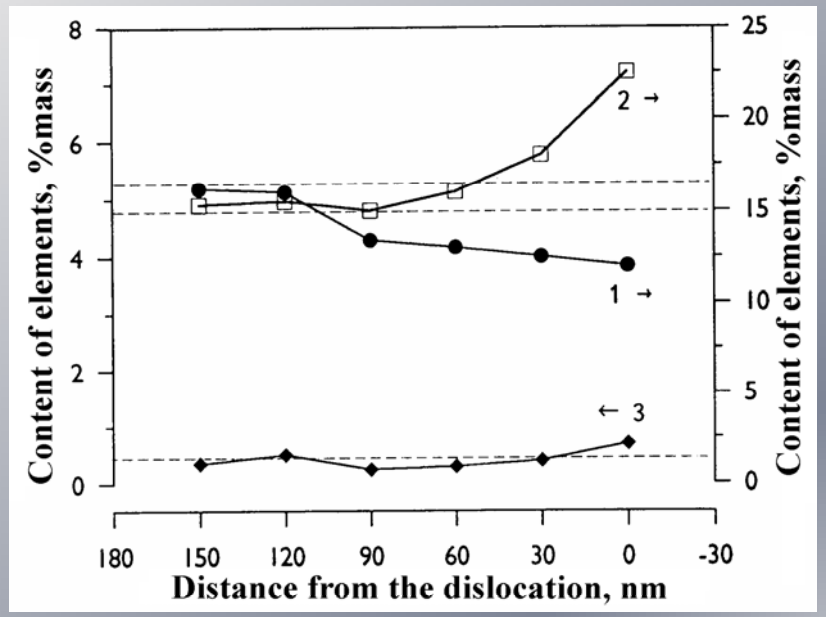

Segregation profile near the large dislocation loop in steel EP-450 (image of the loop is perpendicular to the image plane) (Cr^{3+}, E=4.5 MeV, D=48 dpa, $T_{irr.}$=575°C): 1 – Cr, 2 – Si

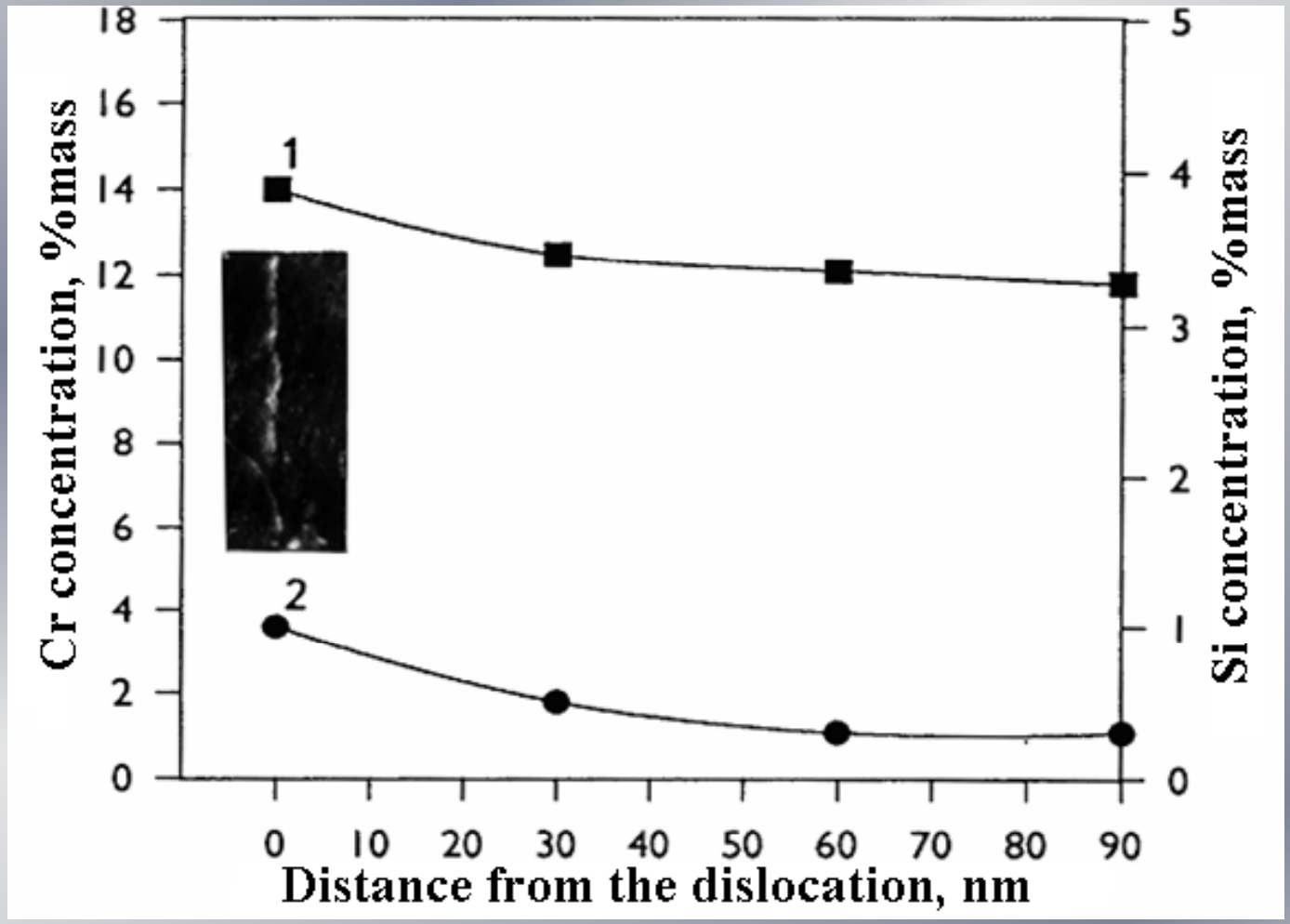

Characteristics of second phase precipitatesprecipitates in irradiated austenitic steels (1)

Phase	Crystalline structure	Number of atoms in elemental cell	Parameter of the lattice	Volume misfit	Base elements	Radiation-induced segregation
γ	Cube Fm3m	1	0,36	-	-	-
Radiation-induced phases						
γ '(M_3Si)	Cube Fm3m, L12	4	0,35	-0,1	Si, Ni, Mn, Mo	High RIS Segregation of Ni, Si depletion of Mo, Cr
G	Cube Fm3m, A1	116	1,102	0,05	Si, Ni	High RIS Segregation of Ni, Si depletion of Mo, Cr
Fe_2P	Hexagonal P321, C22		0,6 (c/a=0,6)	-0,4	P, Si, Ni, Mo, Cr	Mean segregation more intensive or thermal segregation, some depletion of Mo, Cr

Characteristics of precipitates of second phases in irradiated austenitic steels (2)

Radiation induced phases	Crystalline structure	Number of atoms in elemental cell	Parameter of the lattice	Volume misfit	Base elements	Radiation-induced segregation
η- (M6C)	Cube Fd3m, E93	96(82 Me)	1,08	0,1	Mo, Si, Cr, Ni, Fe	Weak segregation
Laves - (Fe2(Mo, Nb))	HexagonalP63/mmc C14	12	0,47 (c0/a0 =0,77)	-0,05	-	
Radiation-modified phases						
($M_{23}C_6$)	Cube Fm3m, D84	92 (73 Me)	1,06	0,1	Cr, Mo, Ti, Fe	RIS is absent Cr, Mo, Si, C segregate
MC	Cube Fm3m, B1	4	0,43	0,7		
σ	Tetragonal P4/mnm, D8B	30	0,88 (c_0/a_0= 0,52)	Of the order 0	-	-
χ	Cube 143m, A12	58	0,89	0,05	-	-

Classification of precipitates

Local variation of composition caused by RIS leads to the decay of solid solution and form the precipitates of two types

Precipitates suppressing the swelling at the expense of accelerated recombination of point defects on interfaces particles-matrix:

- MC (principally TiC, NbC, VC), Fe_2P or Ni_3Ti

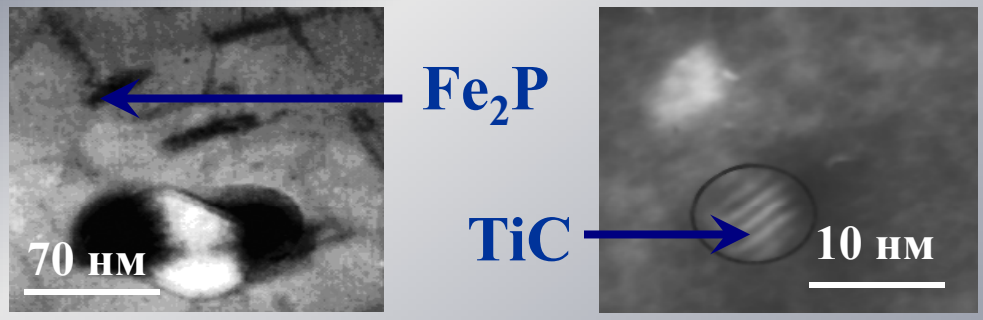

- Precipitates emerging in the result of solid solution decay (especially due to the segregation of Ni and Si) are the sign of the loss of radiation stability on the last stages of the evolution of M_6C structure and G-phase.

γ`-phase in irradiated steel ChS-68 ($Cr^{3+}$, E=3 MeV, D=120 dpa, $T_{irr.}$=580°C a,b) - light-field and dark-field (in the reflection light of γ`-phase) images, respectively; c) electron diffraction pattern, d) characteristic X-ray spectrum from precipitates of γ`-phases

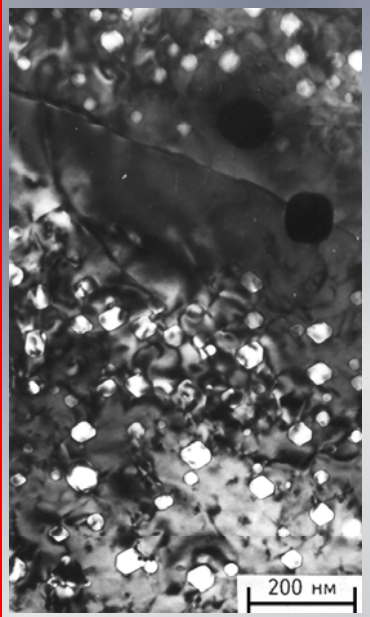

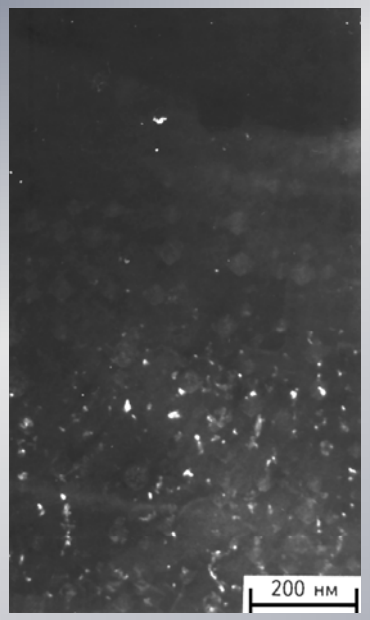

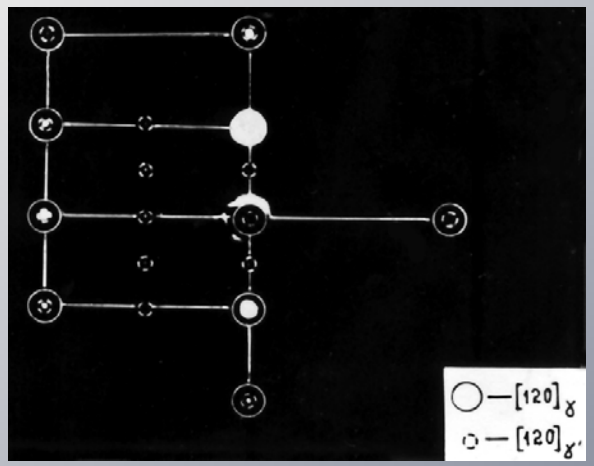

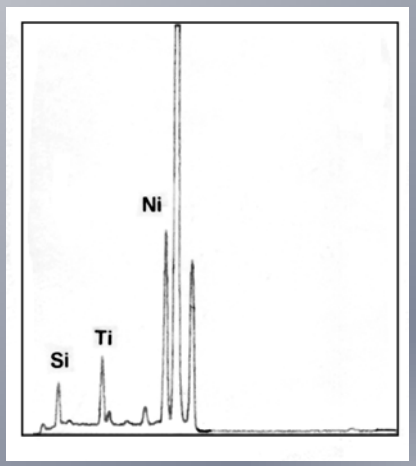

G-phase in ion irradiated steel EI-847 (BOR-60, D=46 dpa, $T_{irr.}$=500°C) a) light field image; b) electron diffraction pattern, c) characteristic X-ray spectrum of precipitates of G-phase

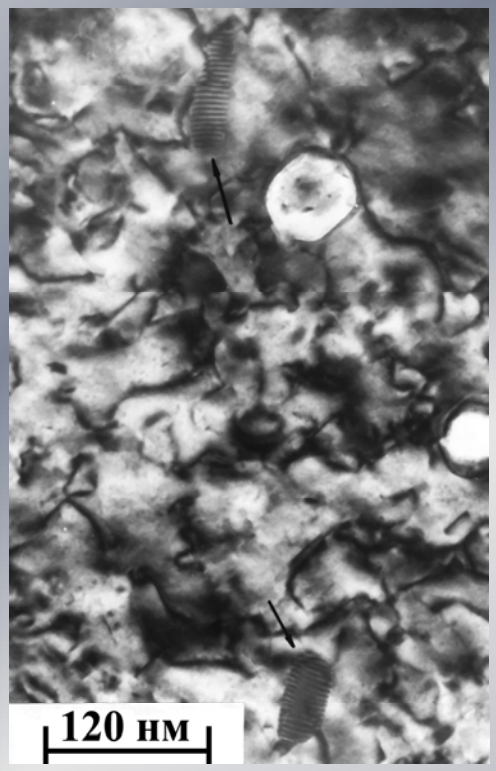

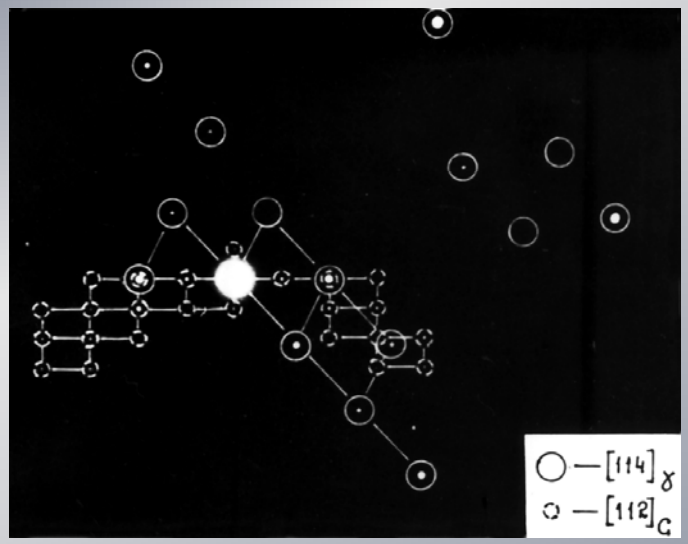

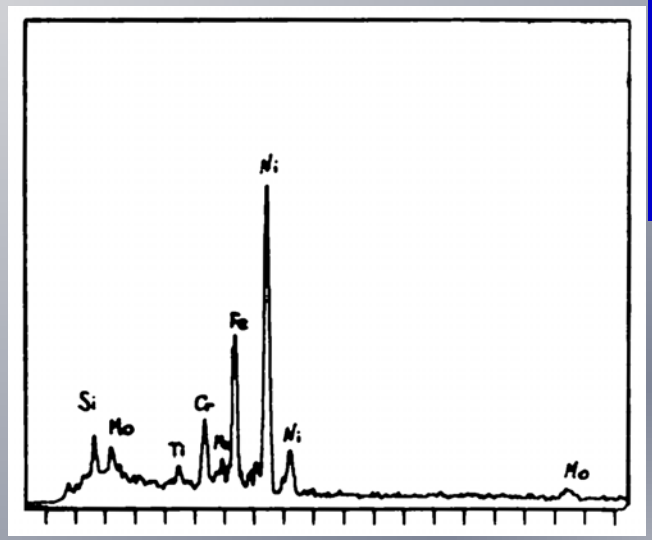

Phosphides in irradiated steel PNC 316 (570°C, 92.5 dpa) a) light field image; b) characteristic X-ray spectrum from precipitate

$(1210)_{ppt}//(011)_{\gamma}$; $(0001)_{ppt}//(001)_{\gamma}$

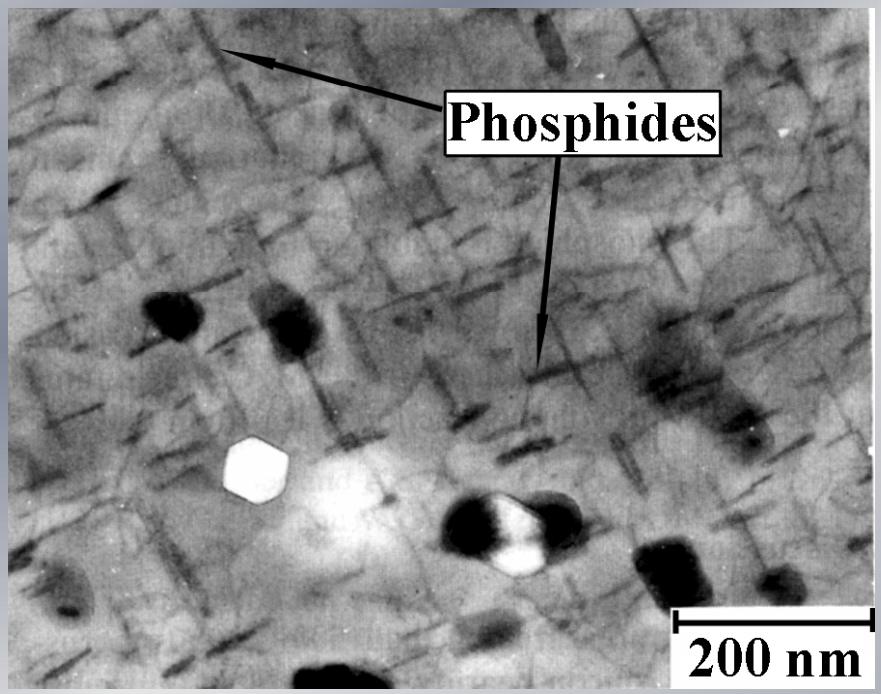

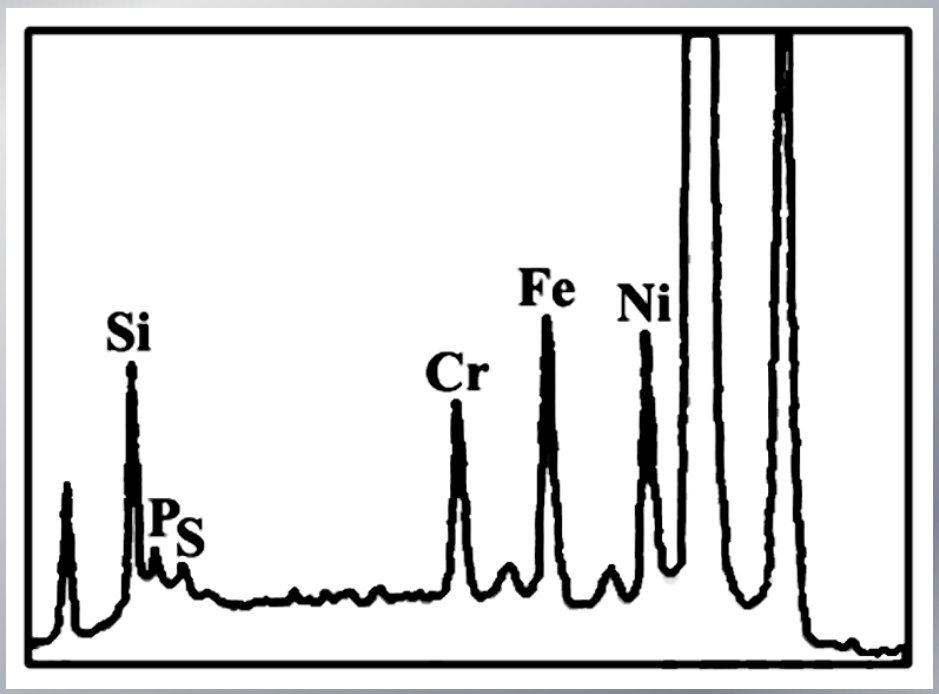

Precipitates MC in steel EI-847(16Cr15Ni3MoNb) a) primary carbidesCr^{3+}, E= 3 MeV, $T_{irr.}$=625^{o}C, D=2 dpa, b) secondary carbides Cr^{3+}, E=3 MeV, $T_{irr.}$= 650^{0}C, D= 2 dpa, c) electron diffraction pattern, d) X-ray spectrum

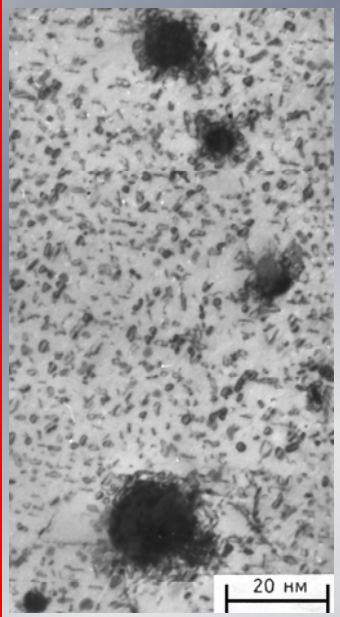

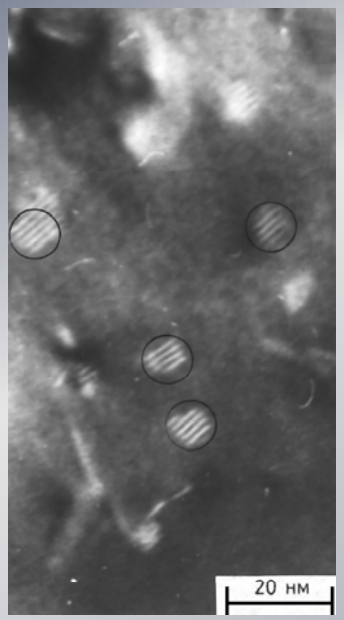

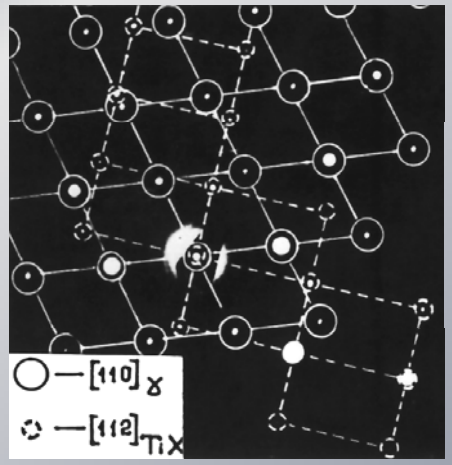

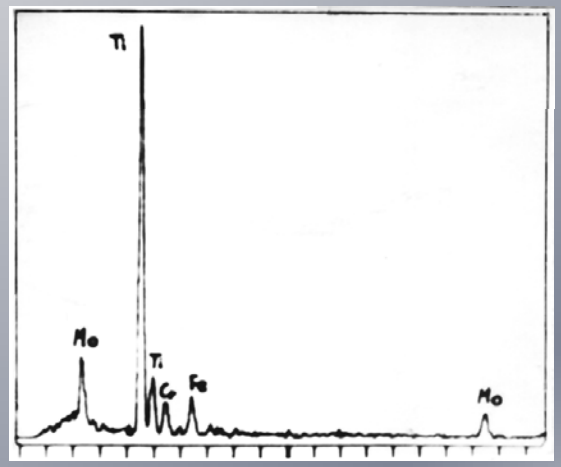

Phases in 20% CW steel AISI 316 after thermal ageing and after irradiation in reactors EBR-II and HFIR (P. Maziasz, 1993)

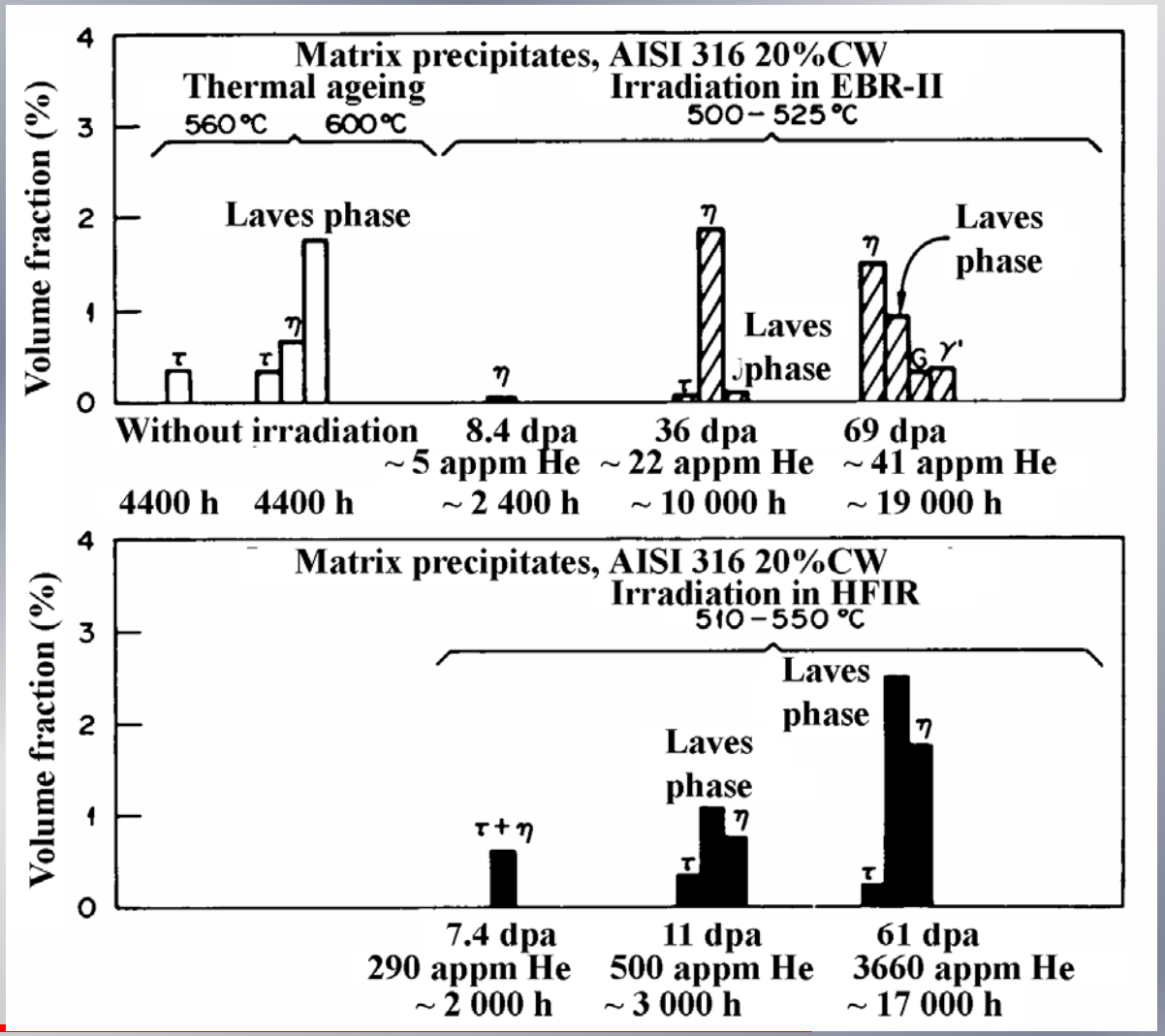

Radiation-induced enrichment by nickel in Laves phases (steel AISI 316, 20% CW) (S. Zinkle, 1993)

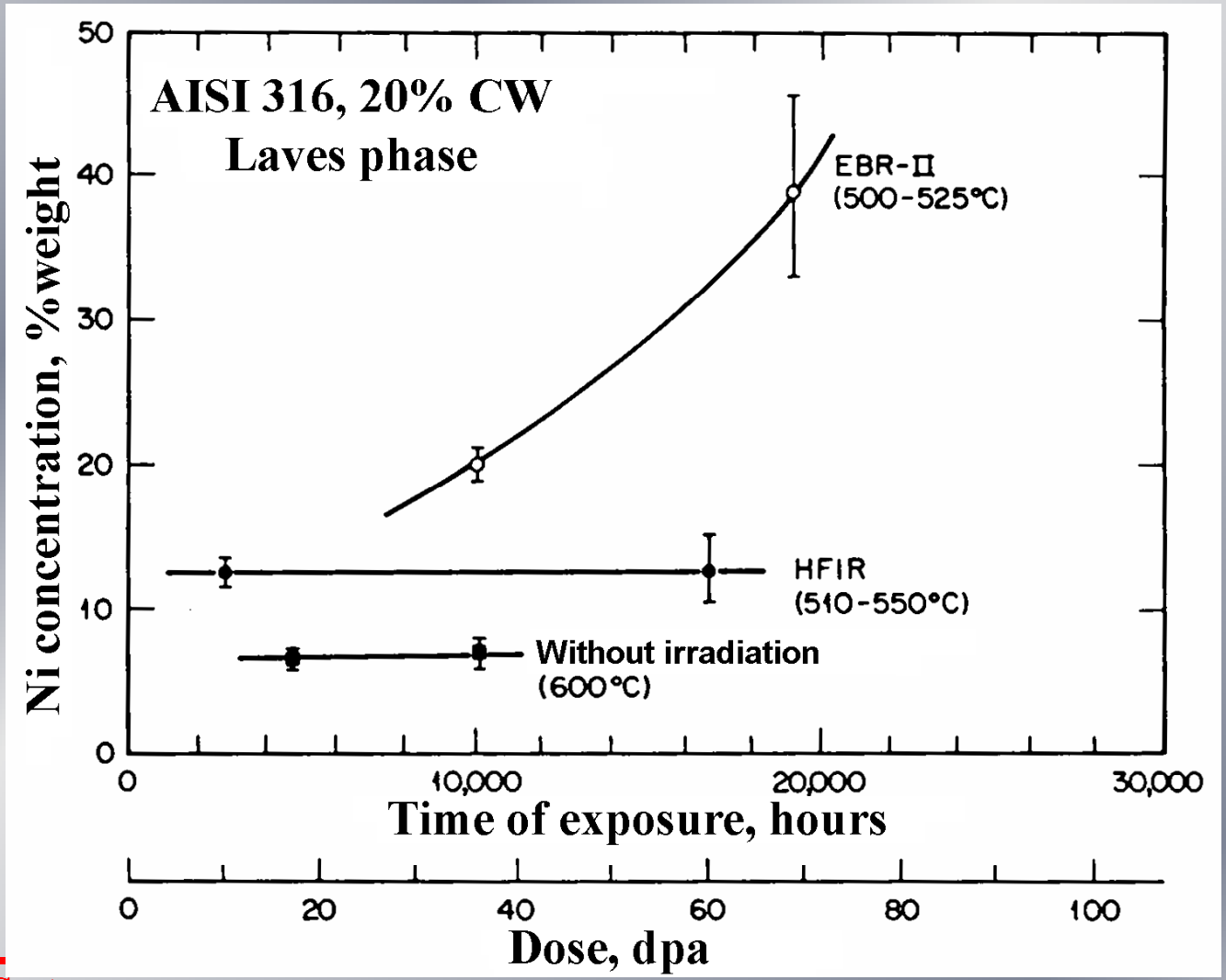

Precipitates behavior in irradiated materials

As a main stage of decay of stainless steels solid solution under irradiation is evolution of second phases precipitates system.

During irradiation second phase precipitates evolution is going.

The evolution of precipitates can go by several ways:

- The precipitates **can grow;**
- The precipitates **can be dissolved;**
- **Infiltration or defiltration of the solid solution elements** can take place (into precipitate from solid solution or from precipitates into solid solution)

Solid solution and precipitates consists closed system which can re exchange their elements, according with their properties, mainly diffusion coefficients and features of the crystal lattice.

Crystalline structure and composition of several phases in irradiated ferritic-martensitic steels

Phase	Crystalline structure	Composition
1. Carbides η- carbides (M_6C) $M_{23}C_6$	Diamond-like	$(Fe_{39}Cr_6Mo_4Si_{10})C$
	Fcc	$(Cr_{14}Fe_{12}Mo_4Si_2WV)C_6$
2 .M_2X MX	hcp	$Cr_2(CN)$, $(CrMo)_2C$, W_2C
	Bcc	NbC, (CrV)N, Nb(CN)
3. Laves phase	Hcp	$Fe_2(Mo,W)$, $Fe_2(Mo,Nb)$, $Fe_2(Mo,Si)$
4. χ- phase	bcc.	$Fe_{35}Cr_{12}Mo_{10}C$
5. α`-phase	Bcc	
6. G- phase	Fcc	Fe_2Mo
8. σ-phase	bct	$Fe_{45}Cr_{30}Mo_{25}$

α` - phase (30%Fe-70%Cr) in steel EP-450 (Cr^{3+}, E=3 MeV, D=150 dpa, $T_{irr.}$=412°C) a) light field image; b) dark field image

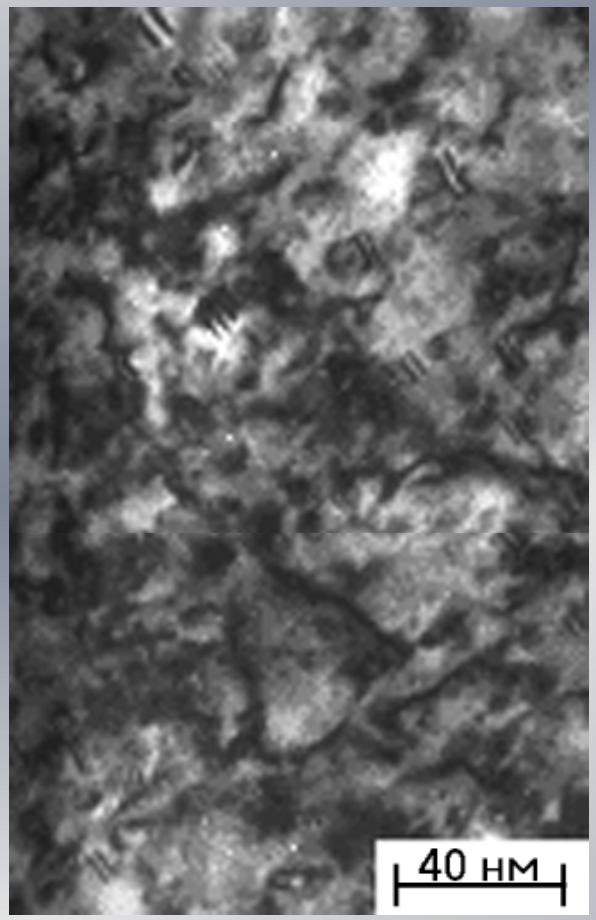

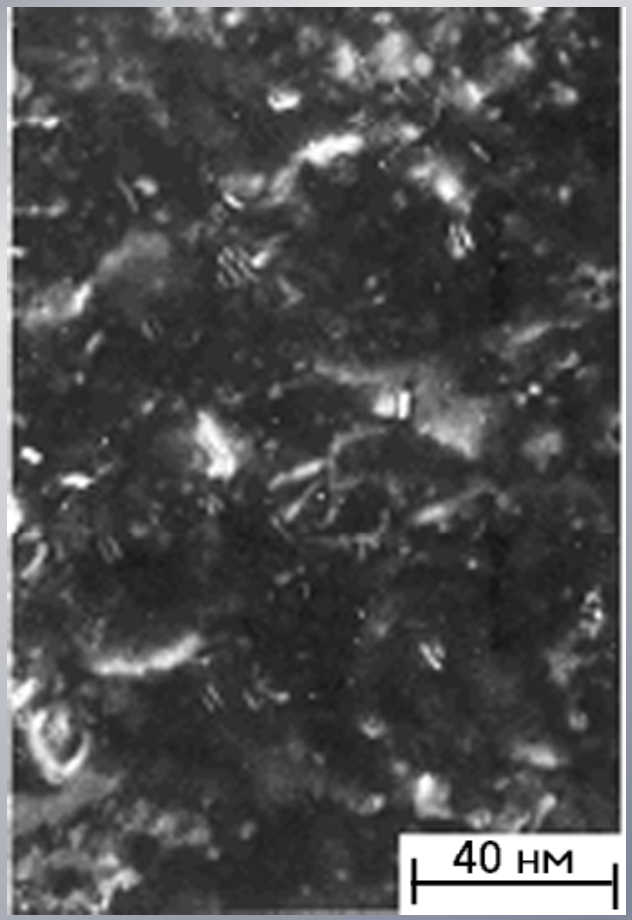

α′-phase formation is common for irradiated F/M steels with 13% Cr content. Very important that in any cases it can serve as radiation-induced phase .

Precipitates of M_2X phase in ferrite (EP-450, Cr^{3+}, E= 3 MeV, D=80 dpa, $T_{ir.}$=510°C) a) bright field image; b) electron diffraction pattern

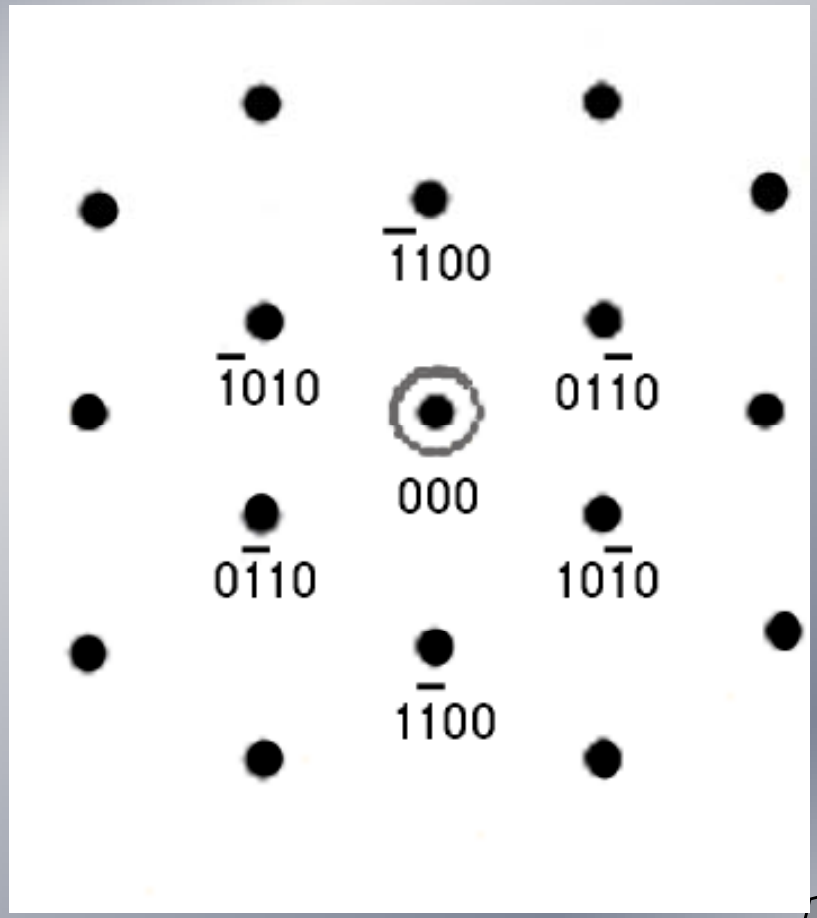

F/ M steels precipitates behaviour

The Cr behaviour in irradiated ferritic steels affects mainly the evolution of the second phase precipitates. We showed that during irradiation 9% and 12% Cr steels to have formation of a few kinds of second-phase precipitates:

- M_6X and $M_{23}C_6$ precipitates are distributed mainly at grain boundaries and did not change their composition during irradiation.
- α′-phase precipitates are predominantly Cr (up to 85–90%), are ≤10 nm in size, and are uniformly distributed through both ferrite and tempered martensite. Most of the precipitates are coherent. Irradiation of lower Cr-content steels (9% to 10% Cr) can also reduce the amount of Cr sufficiently to cause the formation of the α′-phase.
- M_2X precipitates exist in 13% as well in 9% Cr steels. They can have a needle-shaped form (in EP-450 steel) and are finely dispersed (in 9Cr-1Mo-NbVB steel).
- New phase-the formation of Si-enrichment precipitates with stoichiometric compositions (Cr,Fe)9Nb3Si8, as well as the enrichment of Cr_2N and M_6X precipitates with silicon and vanadium, can serve as proof that segregation processes occur in irradiated ferritic steels
- Typical for Laves phases Fe2(Mo,Nb) in 10Cr6MoNbV steel it was founded the phase transformation to χ(Fe36Cr12Mo10) phase according with suggested model of phase transformations.

Structure and composition of second phase, observed in irradiated F-M steels

Phase	Crystallic structure	Composition
1. Carbide	Diamond-like	$(Fe_{39}Cr_6Mo_4Si_{10})C$
η- carbide (M_6C), $M_{23}C_6$	FCC	$(Cr_{14}Fe_{12}Mo_4Si_2WV)C_6$
2 .M_2X	HCP	$Cr_2(CN)$, $(CrMo)_2C$, W_2C
MX	BCC	NbC, (CrV)N, Nb(CN)
3. Laves	HCP	$Fe_2(Mo,W)$, $Fe_2(Mo,Nb)$, $Fe_2(Mo,Si)$
4. χ- phase	BCC	$Fe_{35}Cr_{12}Mo_{10}C$
5. α`- phase	BCC	
6. G- phase	FCC	Fe_2Mo
8. σ- phase	BCC	$Fe_{45}Cr_{30}Mo_{25}$

Phase transformation and phase stability

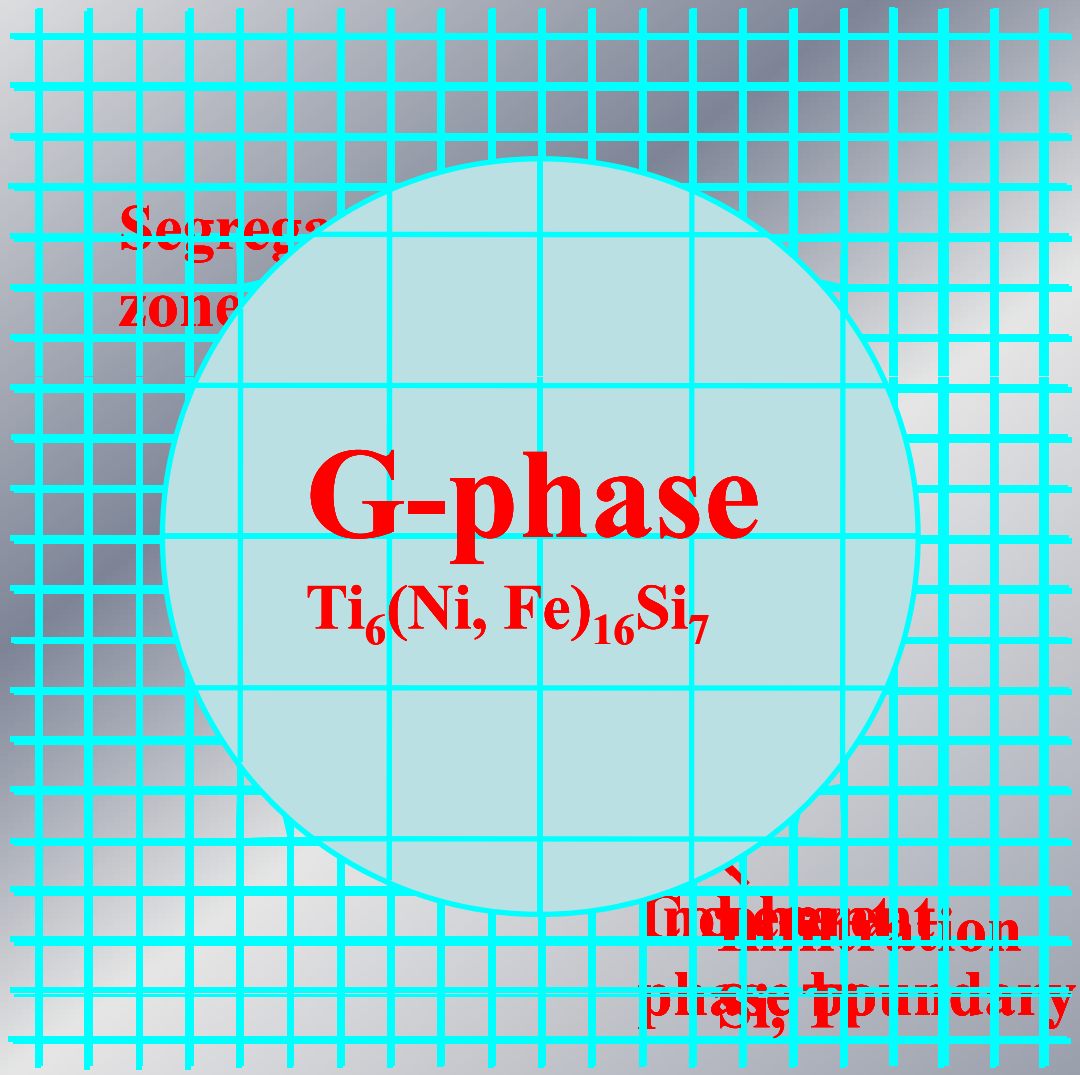

- Nucleation and growth of precipitates with coherent boundaries
- Loss of coherency. Creation on interface sinks of point defects
- Segregation. Elements infiltration from matrix and precipitates on interfaces
- Exceeding of solubility limit. Formation of new precipitates
- More stable precipitates have interface with higher degree of coherency

Typical for spherical FCC precipitates (TiC, NbC, VC etc.)

HCP precipitates according with coherence conditions can or transform to globular - η-phase (Ni_3Ti) or dissolve - (Fe_2P)

Variation of phosphides composition under irradiation

Element, % mass	Fe	Cr	Ni	Mn	P	Si	Sc	Phase
Without irradiation	9,3	3,1	45,1	2,0	11,3	—	31,2	$(Ni,Sc)_2P$
40 dpa	11,2	1,4	41,9	—	8,1	4,2	28,9	$(Ni,Sc)_2P$
100 dpa	12,7	3,3	50,3	2,2	2,9	6,2	12,6	G-phase

Variation of carbides composition under irradiation

Element , % mass	Nb	Mo	Fe	Cr	Ni	Mn	Si	Phase
Without irradiation	99	0,5	0,3	0.2	—	—	—	MC
40 dpa	72	2	10	3	9	—	4	MC
100 dpa	11	3	16	4	51	3	12	G-phase

Diagram of the mechanism of forced infiltration of elements segregating on uncoherent phase boundary;

J^v – flux of vacancies,

$J^v_{k,m}$ –flux of atoms of sort k or m from the boundary by vacancies

$J^i_{k,m}$ –flux of atoms of sort k or m towards the boundary by interstitials.

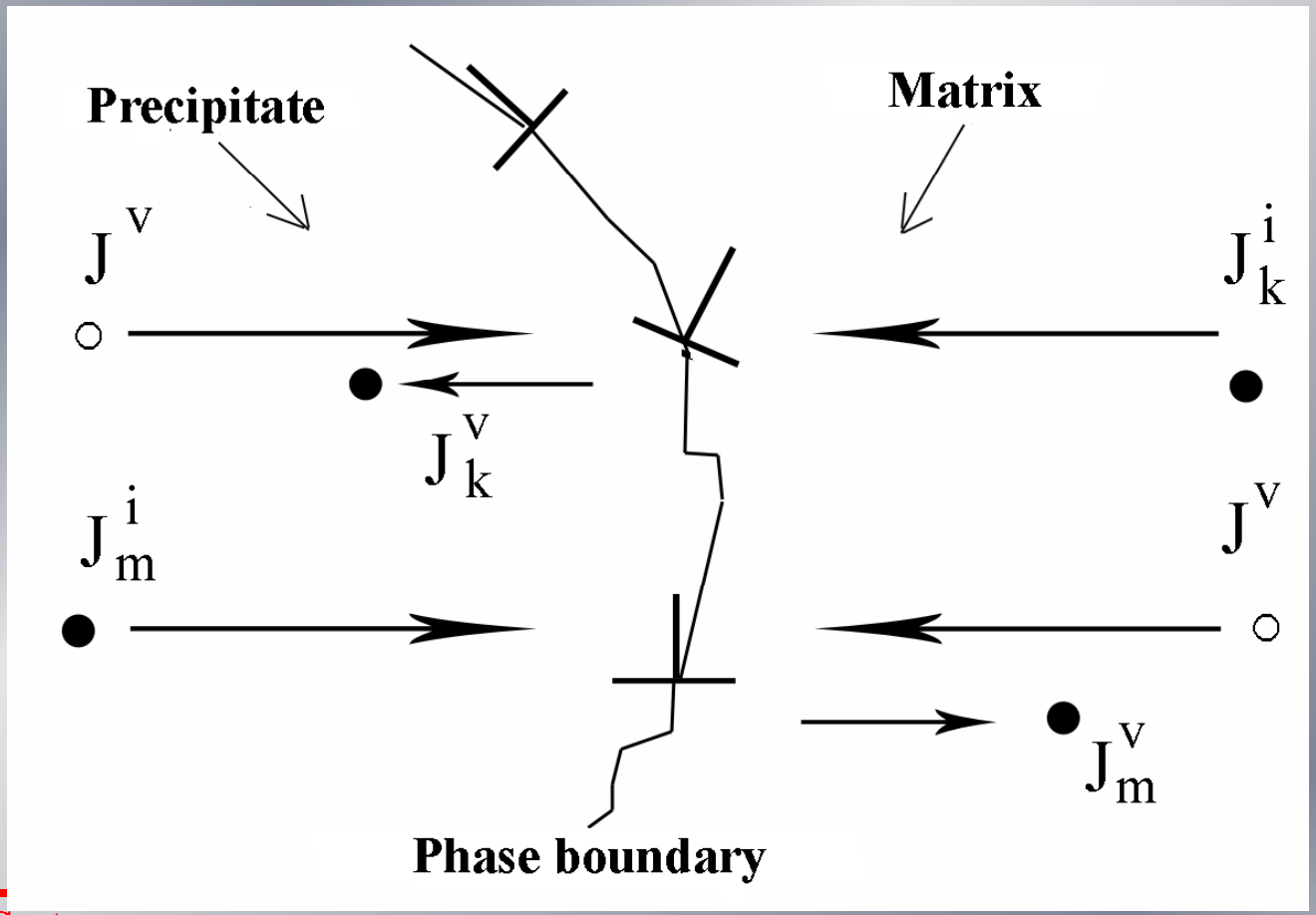

Microstructure of void structure in EI-847 steel (Cr^{3+} E=3MeV, K=10^{-3}dpa/s, D=100 dpa, T_{irr}=625°C
a) SA 1050°C, 30 min;
b) SA 1050°C, 30 min + 10% CW;
c) SA 1050°C, 30 min + 30% CW.

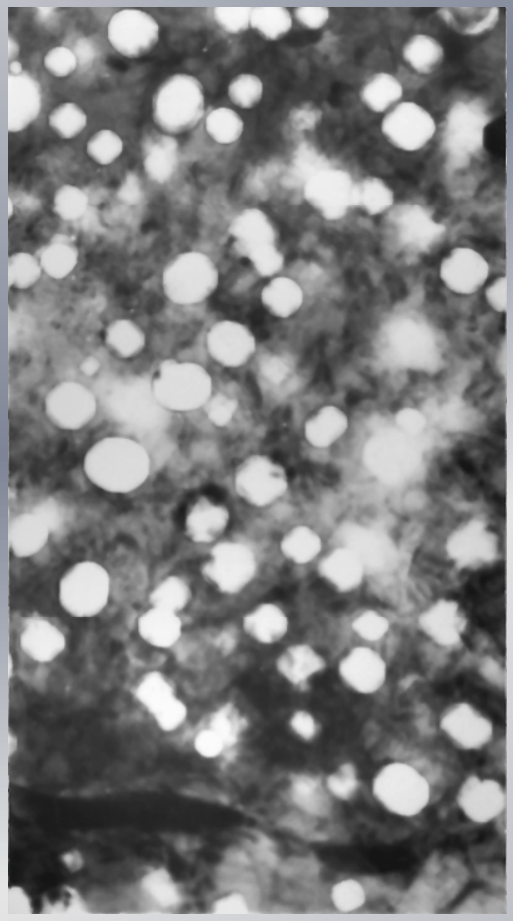

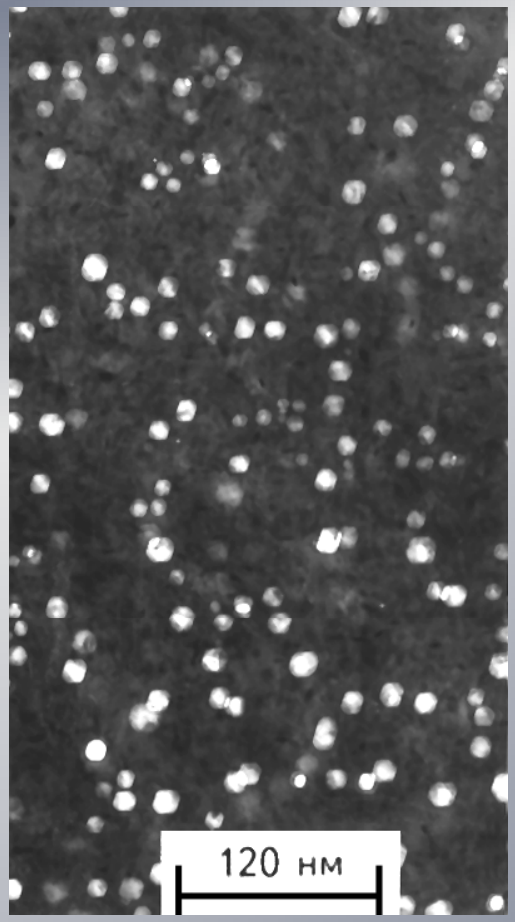

Decay of the solid solution in F-M steels

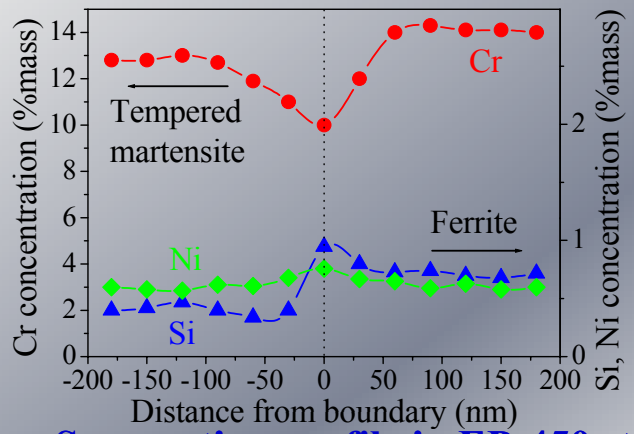

Segregation profile in EP-450 steel (BOR-60, T_{irr}=500°C, D=38 dpa, tempered martensite)

- **Interfacial boundaries (neutral sinks) are enriched by Si and depleted by Cr, Mo, Nb.**

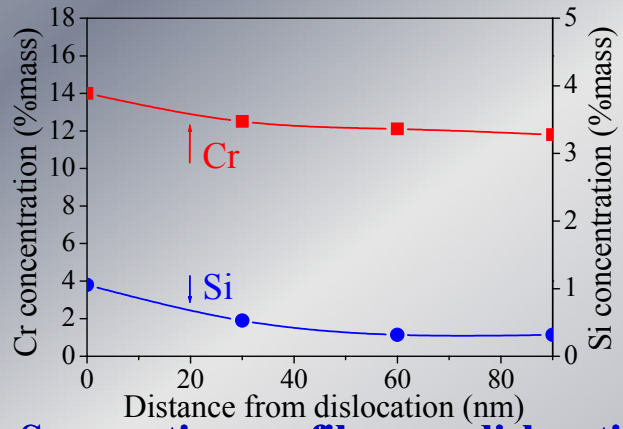

Segregation profile near dislocation loop in EP-450 steel (Cr^{3+}, E=1MeV, T=575^{0}C, D=48dpa)

- **Preferential sinks (interstitial dislocation loops with b=a <100>)-enrichment of Cr and Si take place**

F-M steels precipitates behaviour

The Cr behaviour in irradiated ferritic steels affects mainly the evolution of the second phase precipitates. We showed that during irradiation 9% and 12% Cr steels to have formation of a few kinds of second-phase precipitates:

- M_6X and $M_{23}C_6$ precipitates are distributed mainly at grain boundaries and did not change their composition during irradiation.
- α′-phase precipitates are predominantly Cr (up to 85–90%), are ≤10 nm in size, and are uniformly distributed through both ferrite and tempered martensite. Most of the precipitates are coherent. Irradiation of lower Cr-content steels (9% to 10% Cr) can also reduce the amount of Cr sufficiently to cause the formation of the α′-phase.
- M_2X precipitates exist in 13% as well in 9% Cr steels. They can have a needle-shaped form (in EP-450 steel) and are finely dispersed (in 9Cr-1Mo-NbVB steel).
- New phase-the formation of Si-enrichment precipitates with stoichiometric compositions $(Cr,Fe)_9Nb_3Si_8$, as well as the enrichment of Cr_2N and M_6X precipitates with silicon and vanadium, can serve as proof that segregation processes occur in irradiated ferritic steels
- Typical for Laves phases $Fe_2(Mo,Nb)$ in 10Cr6MoNbV steel it was founded the phase transformation to $\chi(Fe_{36}Cr_{12}Mo_{10})$ phase according with suggested model of phase transformations.

α′-phase formation is common for irradiated F/M steels with 13% Cr content. Very important that in any cases it can serve as radiation-induced phase .

Evaluation of swelling in ferritic-martensitic steel EP-450 (Cr^{+3}, E =3 MeV, T_{irr}=500^{0}C)

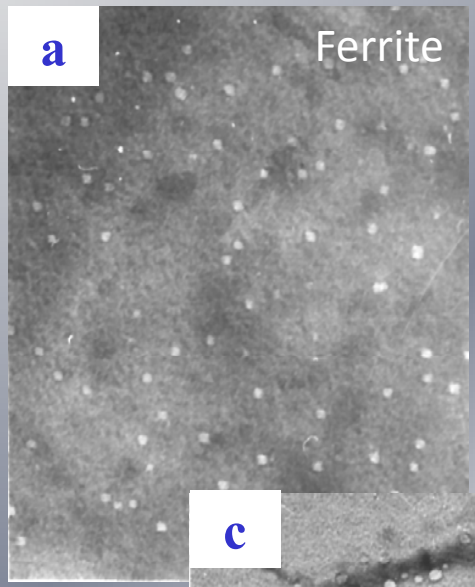

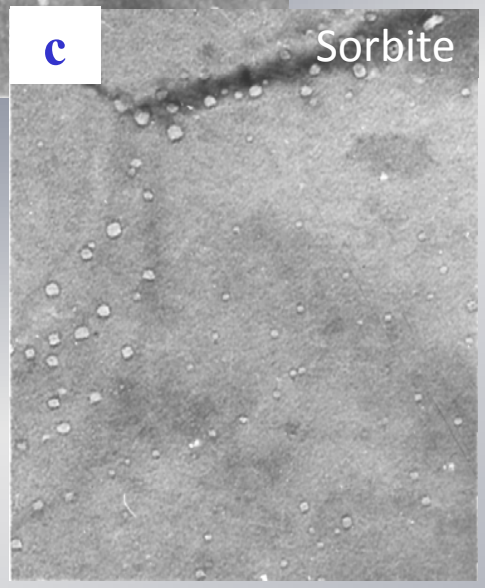

a, c – D=150 dpa

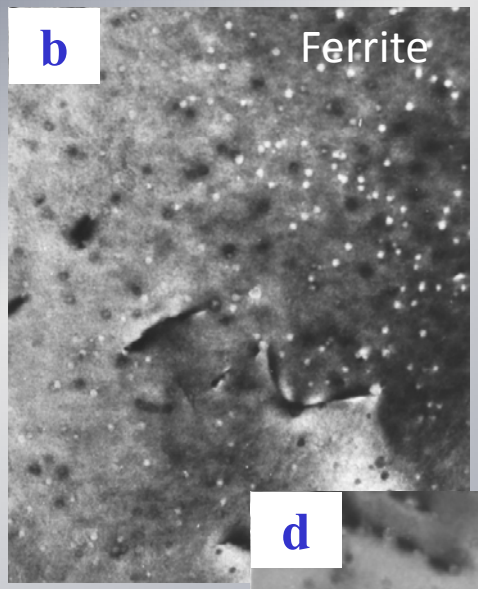

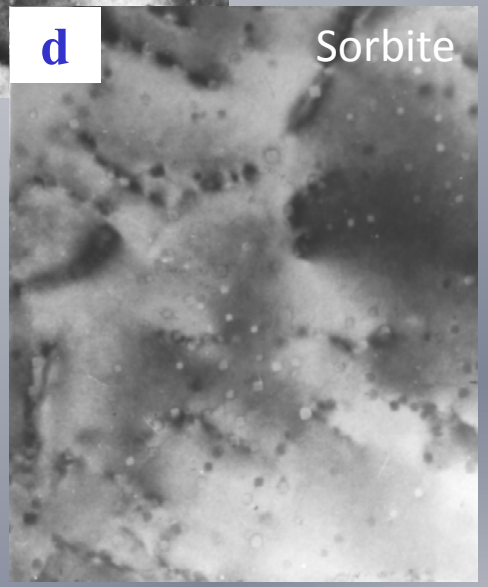

b, d – D=275 dpa

Morphology of voids in irradiated steel 18Cr10NiTi (BOR-60, D=40 dpa, $T_{irr.}$=580°C): a) octahedron voids, associated with G-phase; b) cube voids.

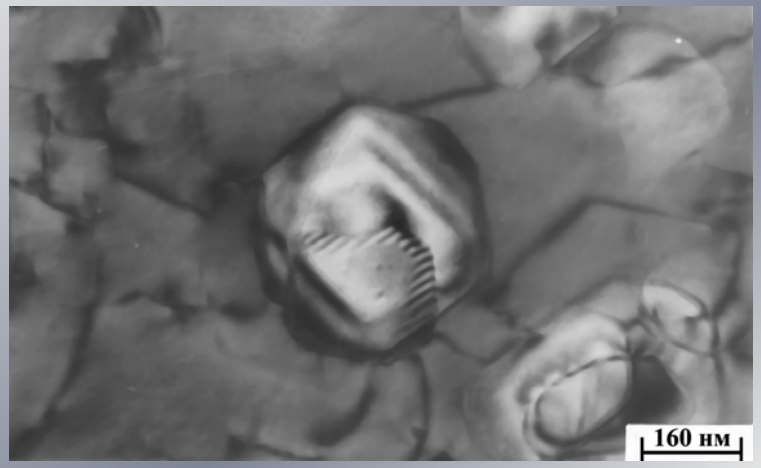

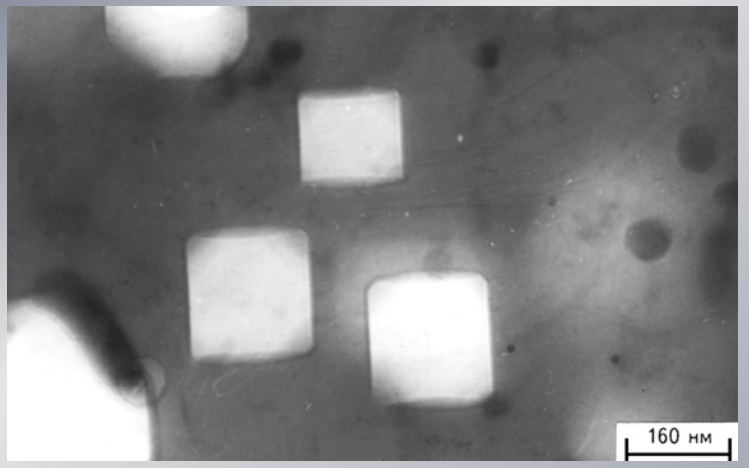

Schematic image of MPC analysis of specimen area:
a) containing isolated void;
b) containing void with the particle of G-phase.

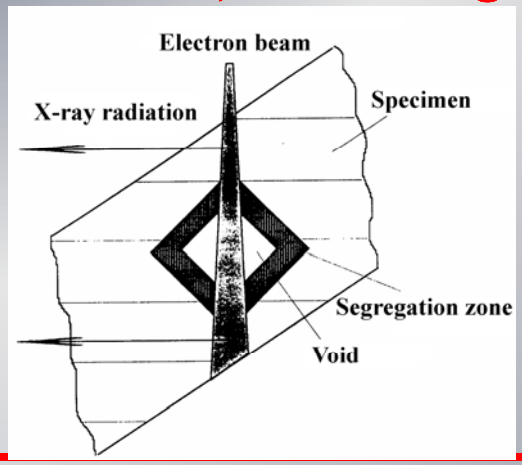

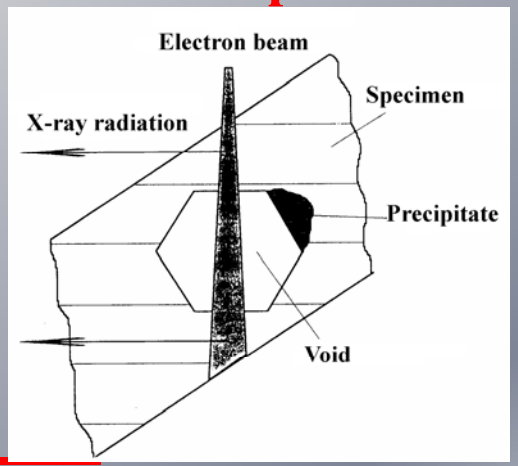

Results of MPC analysis of element composition near cube void

Studied object	Element, mass %						Number of performed experiments
	Si	Ti	Cr	Fe	Ni	Mn	
Matrix	0,3	0,4	21,2	69,8	8,3	–	–
Void without phase	1,2	0,1	16,0	67,9	14,8	–	37
Void with phase	0,2	0,1	20,2	71,4	8,1	–	37
G-phase	12,5	7,7	5,4	10	62	–	46

Concentration profiles of alloying elements along the cube void in neutron irradiated steel 18Cr10NiTi

▲ – Cr, ◊ - Fe, ● – Ni, □ – Ti, ■ – Si

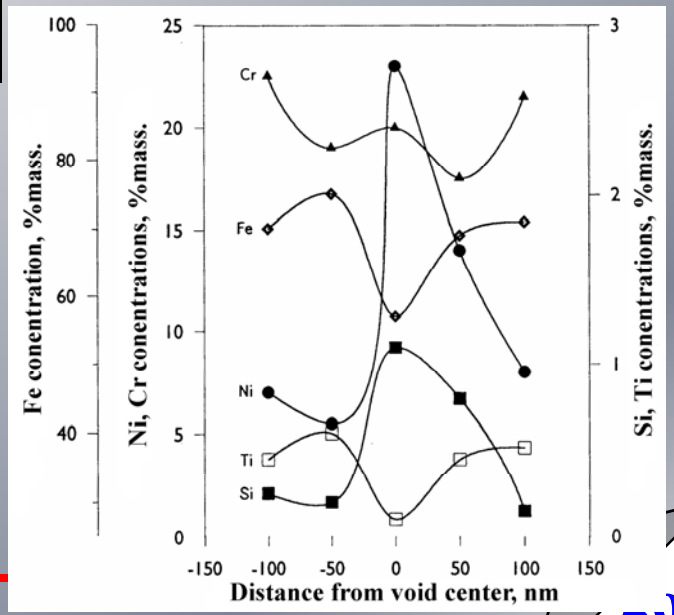

Diagram of cascade-induced dissolution of sphere precipitate

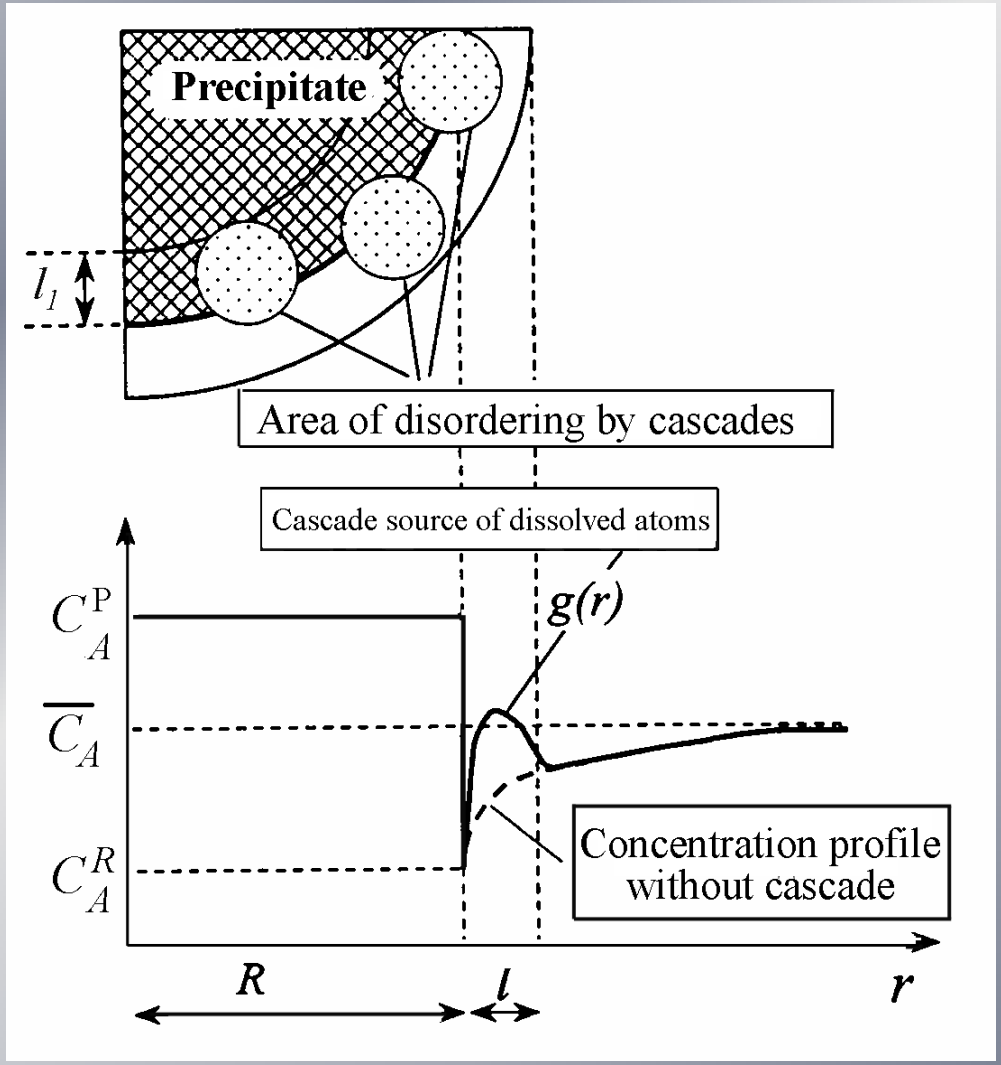

Evolution of η-phase in steel 13Cr13Ni3Ti, irradiated by Cr ions (Cr^{3+}, E=3 MeV, $T_{irr.}$=635°C); a) D=45 dpa; b) D=130 dpa; c) D= 160 dpa

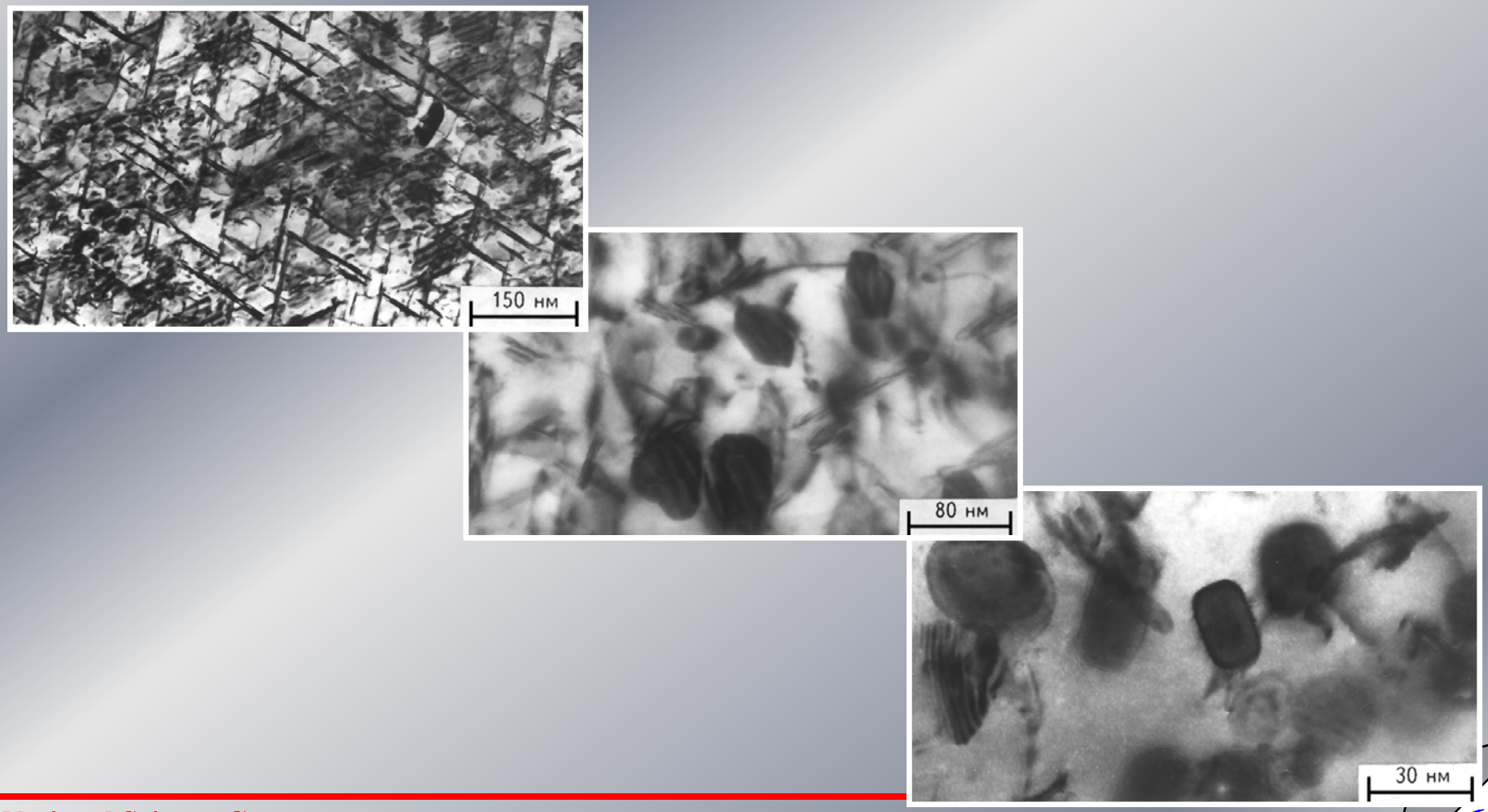

Summary to lecture 2.

It is possible to select the following processes responsible for evolution of microstructure and composition in materials during an irradiation:

- generation of points defects;
- atomic mixing
- dissolution in cascades;
- nucleation of point defects sinks (vacancy and interstitial loops, nuclei of voids);
- evolution of system of sinks (growth of voids and dislocation net);
- radiation-accelerated diffusion (RAD);
- radiation-induced segregation (RIS);
- radiation-induced change (RIC of phase composition)

The majority of these processes in researched experimental conditions operate simultaneously, influencing considerably each other.

The evolution of the materials properties under severe conditions, such as radiation damage, is a multiscale phenomenon, starting at the interaction of the energetic particle with matter (at the piscosecond and nanometre scales) which produces point defects and displacement cascades and leading up to the component evolution (at the year/decade and mascroscopic scales) with formation of large defects or solute clusters and changes of the mechanical properties. The understanding and the prediction of the material evolution require knowledge at the different scales involved to some-how form a complete picture of what is happening.